

# Semiclassical Approach to Photophysics Beyond Kasha’s Rule and Vibronic Spectroscopy Beyond the Condon Approximation. The Case of Azulene

Antonio Prlj,<sup>†,¶</sup> Tomislav Begušić,<sup>†,¶</sup> Zhan Tong Zhang,<sup>†</sup> George Cameron Fish,<sup>‡</sup> Marius Wehrle,<sup>†</sup> Tomáš Zimmermann,<sup>†</sup> Seonghoon Choi,<sup>†</sup> Julien Roulet,<sup>†</sup> Jacques-Edouard Moser,<sup>\*,‡</sup> and Jiří Vaníček<sup>\*,†</sup>

<sup>†</sup>*Laboratory of Theoretical Physical Chemistry, Institut des Sciences et Ingénierie Chimiques, Ecole Polytechnique Fédérale de Lausanne (EPFL), CH-1015, Lausanne, Switzerland*

<sup>‡</sup>*Photochemical Dynamics Group, Institut des Sciences et Ingénierie Chimiques, Ecole Polytechnique Fédérale de Lausanne (EPFL), CH-1015, Lausanne, Switzerland*

<sup>¶</sup>*These authors contributed equally.*

E-mail: je.moser@epfl.ch; jiri.vanicek@epfl.ch

## Abstract

Azulene is a prototypical molecule with an anomalous fluorescence from the second excited electronic state, thus violating Kasha’s rule, and with an emission spectrum that cannot be understood within the Condon approximation. To better understand photophysics and spectroscopy of azulene and other non-conventional molecules, we develop a systematic, general, and efficient computational approach combining semi-classical dynamics of nuclei with ab initio electronic structure. First, to analyze the nonadiabatic effects, we complement the standard population dynamics by a rigorous

measure of adiabaticity, estimated with the multiple-surface dephasing representation. Second, we propose a new semiclassical method for simulating non-Condon spectra, which combines the extended thawed Gaussian approximation with the efficient single-Hessian approach.  $S_1 \leftarrow S_0$  and  $S_2 \leftarrow S_0$  absorption and  $S_2 \rightarrow S_0$  emission spectra of azulene, recorded in a new set of experiments, agree very well with our calculations. We find that accuracy of the evaluated spectra requires the treatment of anharmonicity, Herzberg–Teller, and mode-mixing effects.

## 1 Introduction

Azulene molecule is an archetypal system violating Kasha’s rule,<sup>1,2</sup> according to which “polyatomic molecular entities luminesce with appreciable yield only from the lowest excited state of a given multiplicity.”<sup>3</sup> As a result, azulene has attracted significant experimental<sup>4–12</sup> and theoretical<sup>9,10,13–18</sup> attention over the decades. More recently, rigorous experimental and theoretical approaches proved useful in identifying, but also refuting, the violation of Kasha’s rule in other molecular systems.<sup>19–23</sup>

Spectroscopic and photophysical studies tried to explain why observed fluorescence in azulene occurs from the second ( $S_2$ ) instead of the first ( $S_1$ ) excited singlet state. The measured lifetimes of the  $S_1$  state of azulene range from  $\sim 2$  ps in solution<sup>4</sup> to  $\sim 1$  ps in the gas phase,<sup>5,7</sup> indicating that radiationless decay is much faster than the time scale of emission itself. Surface-hopping and Ehrenfest simulations by Robb *et al.*<sup>13,14</sup> ascribed the ultrafast decay to the energetically low-lying conical intersection (see Fig. 1) between the  $S_1$  state and the ground electronic state,  $S_0$ , although the estimated  $S_1$  lifetime ( $\sim 10$  fs) was significantly smaller than the experimental one. Apart from the  $S_1$  fluorescence quenching, which is ubiquitous in a wide range of small and medium-sized organic molecules, anomalous behavior of azulene shows itself in the characteristic fluorescence from the  $S_2$  state. Hindered  $S_2 \rightarrow S_1$  internal conversion is attributed to the wide interstate gap (see Fig. 1) and, more precisely, to the weak nonadiabatic coupling (NAC), giving rise to the moderate, yet distinctive,  $S_2$

emission. It was estimated that fluorescence quantum yield  $\Phi_f(S_2)$  of the second excited state outcompetes  $\Phi_f(S_1)$  by four orders of magnitude, while the nonradiative internal conversion constant  $k_{IC}^{2 \rightarrow 1}$  is 100 times smaller than  $k_{IC}^{1 \rightarrow 0}$ .<sup>15</sup> The  $S_1 \leftarrow S_0$  absorption spectrum was correctly reproduced by Franck-Condon simulations,<sup>24,25</sup> assuming the validity of Condon approximation,<sup>26</sup> which neglects the dependence of the transition dipole moment on nuclear coordinates. The most comprehensive study of importance of non-Condon effects in azulene was the early work of Gustav and Storch,<sup>15</sup> who showed that  $S_1$  absorption and emission have dominant Condon contributions, while  $S_2 \rightarrow S_0$  emission has important Herzberg-Teller effects.  $S_2 \leftarrow S_0$  absorption was not considered.

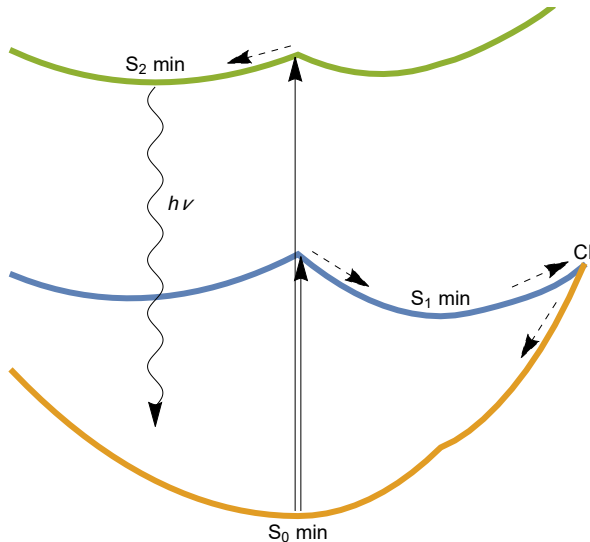


Figure 1: Schematic representation of azulene photophysics involving  $S_1$  (right) and  $S_2$  state (left). Absorption, emission, and nuclear dynamics are represented by full, curved, and dashed arrows, respectively. Potential energy surface cuts are based on CASSCF electronic structure (see Supporting Information for details). Note that the calculations of adiabaticity, population dynamics, and spectra presented in the results section are based on full-dimensional ab initio potential energy surfaces and not on this schematic representation.

Motivated by its unusual photophysics and spectroscopy, we use azulene as a test case for introducing an efficient computational approach for studying various Kasha violating (or Kasha-obeying) systems. Such theoretical tool seems necessary since experimental verification of anti-Kasha behavior may be quite challenging, as demonstrated by recent reports.<sup>22,23</sup> The proposed methodology consists of two steps: (i) To analyze the influence of NACs on

the excited-state dynamics, we evaluate the “adiabaticity” with a rigorous measure that is approximately evaluated semiclassically with the multiple-surface dephasing representation (MSDR).<sup>27,28</sup> Because it can detect more subtle nonadiabatic effects, the adiabaticity goes beyond the standard analysis based on population dynamics.<sup>29–38</sup> (ii) Building on the joint analysis of adiabaticity and population dynamics, we introduce a new method for computing vibrationally resolved electronic spectra by combining the single-Hessian<sup>39</sup> and extended<sup>40–42</sup> thawed Gaussian approximations. The new methodology, augmented with on-the-fly *ab initio* electronic structure calculations, is applied to study nonadiabatic, non-Condon, anharmonicity, and mode-mixing effects in the first two excited states of azulene.

## 2 Theory

### 2.1 Measuring adiabaticity with multiple-surface dephasing representation

A natural way to estimate the effect of NACs on the molecular quantum dynamics launched from a certain electronic state is to analyze the subsequent population dynamics. In higher dimensions, the time dependence of populations is most often approximated with mixed quantum-classical methods, in which the molecular wavefunction  $\Psi$  is replaced with an ensemble of  $N$  trajectories, each of which is characterized by the classical nuclear position ( $q$ ) and momentum ( $p$ ), propagated with Hamilton’s equations of motion,

$$\dot{q}_j(t) = \frac{\partial H^{(j)}(q_j, p_j)}{\partial p_j}, \quad \dot{p}_j(t) = -\frac{\partial H^{(j)}(q_j, p_j)}{\partial q_j}, \quad (1)$$

and by the electronic wavefunction  $\mathbf{c}$ , propagated with the time-dependent Schrödinger equation

$$i\hbar\dot{\mathbf{c}}_j(t) = \mathbf{H}(q_j(t), p_j(t))\mathbf{c}_j(t). \quad (2)$$

Here  $j = 1, \dots, N$  is the index of the trajectory,  $H^{(j)}$  is a method-dependent approximate Hamiltonian associated with the  $j$ th trajectory, and  $\mathbf{H}$  denotes the fully coupled molecular Hamiltonian expressed in the basis of the  $S$  considered electronic states. In general, the bold face denotes either the  $S$ -component vectors (e.g.,  $\mathbf{c}$ ) or  $S \times S$  matrices (e.g.  $\mathbf{H}$ ) acting on the Hilbert space spanned by the  $S$  electronic states. While Ehrenfest dynamics evolves  $q$  and  $p$  with the locally mean-field Hamiltonian  $H_{\text{Ehr}}^{(j)} := \langle \mathbf{H}(q_j(t), p_j(t)) \rangle_{\mathbf{c}_j(t)}$ , where  $\langle \mathbf{A} \rangle_{\mathbf{c}} := \mathbf{c}^\dagger \mathbf{A} \mathbf{c}$  denotes the expectation value of electronic operator  $\mathbf{A}$  in the state  $\mathbf{c}$ , both Born–Oppenheimer and surface hopping<sup>43</sup> algorithms employ the (diagonal) Born–Oppenheimer Hamiltonian  $H_{\text{BO}}^{(j)} \equiv H_{\text{SH}}^{(j)} := \mathbf{H}_{n_j(t)n_j(t)}^{\text{BO}}(q_j(t), p_j(t))$ , where  $n_j(t) \in \{1, \dots, S\}$  is the index of the adiabatic potential energy surface on which the trajectory runs. In addition, in surface hopping, a stochastic algorithm<sup>43</sup> is used to switch (or keep fixed) the current surface  $n_j(t)$  according to the current value of  $\mathbf{c}_j(t)$ , and a so-called “decoherence correction”<sup>44</sup> is frequently added to improve the accuracy and consistency between the populations obtained from the electronic wavefunctions  $\mathbf{c}_j$  (“quantum populations”) and from the histogram of  $n_j$  (“classical populations”).

However, the NACs may affect more than just the populations of different electronic states. A more rigorous measure of the importance of NACs is, therefore, the “adiabaticity,”

$$A(t) := |a(t)|^2, \quad (3)$$

where

$$a(t) = \langle \Psi(t) | \Psi^{\text{BO}}(t) \rangle \quad (4)$$

is the overlap of molecular wavefunctions propagated either exactly or within the Born–Oppenheimer approximation.<sup>27,45,46</sup> More precisely,  $|\Psi(t)\rangle = e^{-i\hat{\mathbf{H}}t/\hbar}|\Psi(0)\rangle$ , where  $\hat{\mathbf{H}}$  is the fully coupled nonadiabatic molecular Hamiltonian and  $|\Psi^{\text{BO}}(t)\rangle = e^{-i\hat{\mathbf{H}}^{\text{BO}}t/\hbar}|\Psi(0)\rangle$ , where  $\hat{\mathbf{H}}^{\text{BO}}$  is the Born–Oppenheimer Hamiltonian, in which the NACs are neglected. The hat  $\hat{\phantom{x}}$  denotes nuclear operators. Obviously, for two normalized wave packets, the adiabaticity

$A$  is a number between 0 and 1, where high adiabaticity,  $A(t) \approx 1$ , indicates that the Born-Oppenheimer approximation at time  $t$  is accurate, whereas low adiabaticity,  $A(t) \ll 1$ , suggests that nonadiabatic couplings are important and should be taken into account in an accurate simulation.

Evaluating adiabaticity  $A(t)$  exactly in higher-dimensional systems is a formidable, if not impossible, task because it requires exact quantum propagation. Fortunately, the semiclassical MSDR provides, in many situations, a very good estimate of adiabaticity at the fraction of the cost of exact quantum calculation.<sup>27,28</sup> Moreover, this semiclassical estimate of adiabaticity amplitude  $\langle \Psi(t) | \Psi^{\text{BO}}(t) \rangle$  is, typically, much more accurate than the semiclassical approximations to the wavefunctions  $\Psi(t)$  and  $\Psi^{\text{BO}}(t)$  themselves. Within the MSDR, the adiabaticity amplitude  $a$  is approximated as

$$a_{\text{MSDR}}(t) = h^{-D} \text{Tr}_e \int dx \rho_W^{\text{init}}(x) \mathcal{T} e^{i \int_0^t \Delta \mathbf{H}_W^I(x, t') dt' / \hbar}, \quad (5)$$

where  $D$  is the number of nuclear degrees of freedom,  $\text{Tr}_e$  denotes the trace over electronic degrees of freedom (the  $S$  electronic states here),  $x = (q, p)$  denotes the  $2D$  nuclear phase space coordinates at time  $t$ , and  $\mathcal{T}$  is the time ordering operator. In addition,  $\rho^{\text{init}}$  is a density operator of the initial state,  $\Delta \hat{\mathbf{H}} := \hat{\mathbf{H}} - \hat{\mathbf{H}}^{\text{BO}}$  is the difference between the exact and Born-Oppenheimer Hamiltonians, superscript  $I$  denotes the interaction picture, and subscript  $W$  indicates a partial Wigner transform<sup>27</sup> over nuclear degrees of freedom. In the most common case of electronically pure states,<sup>27</sup> the MSDR of adiabaticity can be evaluated simply as<sup>27</sup>

$$a_{\text{MSDR}}(t) = \overline{\mathbf{c}(t)^\dagger \mathbf{c}_{\text{BO}}(t)}, \quad (6)$$

where the overbar denotes an average over the ensemble of trajectories,  $\overline{A} := N^{-1} \sum_{j=1}^N A_j$ , while  $\mathbf{c}_{\text{BO}}(t)$  is the electronic wavefunction propagated with Eq. (2) in which the full Hamiltonian  $\mathbf{H}$  is replaced with  $\mathbf{H}^{\text{BO}}$ . As for the nuclear trajectories  $(q, p)$ , they can be propagated with the fewest-switches surface hopping, Ehrenfest, or Born-Oppenheimer dynamics. Over-

all, the MSDR allows quantitative analysis of the importance of NACs (and beyond<sup>47</sup>), adding little additional cost to the (classical) nuclear dynamics itself, while approximately introducing nuclear quantum effects.<sup>27</sup>

## 2.2 Vibrationally resolved electronic spectroscopy

The usual time-dependent approach to one-photon spectroscopy<sup>48</sup> treats the light-matter interaction within the first-order perturbation theory. While it is equivalent to the time-independent Franck–Condon approach, the time-dependent approach unravels the direct relationship between vibrationally resolved electronic spectra and molecular wavepacket dynamics. In the zero-temperature limit, i.e., assuming only the state  $|1, g\rangle$ , the ground ( $g$ ) vibrational state of the ground (1) electronic state, is populated before the interaction with the electromagnetic field, the linear absorption cross-section can be evaluated as<sup>25,48–50</sup>

$$\sigma^{\text{abs}}(\vec{\epsilon}, \omega) = \frac{4\pi\omega}{\hbar c} \text{Re} \int_0^\infty dt C(\vec{\epsilon}, t) e^{i(\omega + \omega_{1,g})t}. \quad (7)$$

Here

$$C(\vec{\epsilon}, t) = \langle \phi(0) | \phi(t) \rangle \quad (8)$$

is the wavepacket autocorrelation function for the initial nuclear wavepacket  $|\phi(0)\rangle = \hat{\mu}|1, g\rangle$  evolved with the excited-state nuclear Hamiltonian  $\hat{H}_2$ ,  $\hat{\mu}$  is the transition dipole moment matrix element  $\hat{\mu}_{21}$  projected on the three-dimensional polarization unit vector  $\vec{\epsilon}$  of the electric field, i.e.,  $\hat{\mu} = \hat{\mu}_{21} \cdot \vec{\epsilon}$ , and  $\hbar\omega_{1,g} = \langle 1, g | \hat{H}_1 | 1, g \rangle$  is the zero point energy. Emission spectrum, expressed as the emission rate per unit frequency, is computed similarly,<sup>25,50</sup> as

$$\sigma^{\text{em}}(\vec{\epsilon}, \omega) = \frac{4\omega^3}{\pi\hbar c^3} \text{Re} \int_0^\infty dt C(\vec{\epsilon}, t)^* e^{i(\omega - \omega_{2,g})t}, \quad (9)$$

where the autocorrelation function  $C(\vec{\epsilon}, t)$  is still given by Eq. (8), but the initial state  $|\phi(0)\rangle = \hat{\mu}|2, g\rangle$ , obtained by multiplying the ground ( $g$ ) vibrational state of an excited (2)

electronic state by the transition dipole moment, is propagated on the ground-state surface. Finally, the spectrum averaged over all molecular orientations is evaluated simply as<sup>42,51</sup>  $\sigma_{\text{av.}}(\omega) = (1/3) \sum_i \sigma(\vec{e}_i, \omega)$ , where  $\vec{e}_i$  ( $i = x, y, z$ ) denotes the unit vector along the  $i$ -axis.

Different methods exist for simulating vibrationally resolved absorption and emission spectra of polyatomic molecules. The most standard approach is based on constructing global harmonic models<sup>52–57</sup> for the ground- and excited-state potential energy surfaces, which requires only a few *ab initio* calculations. The main advantages of the harmonic approximation are the existence of analytical expressions for the autocorrelation functions and the straightforward incorporation of temperature effects at nearly no additional cost. However, the method neglects potentially significant anharmonicity effects.

In an earlier work in our group,<sup>47,58</sup> we showed that the semiclassical MSDR, after a small extension, could be used to approximate vibronic spectra, including nonadiabatic effects, but missing high resolution features. In contrast, the thawed Gaussian approximation,<sup>59</sup> is rather accurate at reproducing moderately resolved vibronic spectra,<sup>41,42,60,61</sup> but cannot account for the nonadiabatic effects. As a result, the thawed Gaussian propagation is limited to systems in which the Born–Oppenheimer approximation holds; in such systems, however, it consistently outperforms commonly used global harmonic methods because it can partially account for the anharmonicity of the potential energy surface.

### 2.3 Evaluating spectra beyond Condon and harmonic approximations with single-Hessian extended thawed Gaussian approximation

The thawed Gaussian approximation propagates a Gaussian wavepacket

$$\psi(q, t) = \frac{1}{(\pi\hbar)^{D/4} \sqrt{\det Q_t}} \exp \left\{ \frac{i}{\hbar} \left[ \frac{1}{2} (q - q_t)^T \cdot P_t \cdot Q_t^{-1} \cdot (q - q_t) + p_t^T \cdot (q - q_t) + S_t \right] \right\}, \quad (10)$$



here written using Hagedorn's parametrization,<sup>62–65</sup> in an effective time-dependent potential given by the local harmonic approximation

$$V_{\text{LHA}}(q, t) = V(q_t) + V'(q_t)^T \cdot (q - q_t) + \frac{1}{2}(q - q_t)^T \cdot V''(q_t) \cdot (q - q_t) \quad (11)$$

of the true potential  $V(q)$  around the center of the wavepacket. In Eq. (10),  $q_t$  and  $p_t$  are the expectation values of position and momentum,  $S_t$  is the classical action, and  $Q_t$  and  $P_t$  are  $D \times D$  complex matrices satisfying the relations<sup>39,63–66</sup>

$$Q_t^T \cdot P_t - P_t^T \cdot Q_t = 0, \quad (12)$$

$$Q_t^\dagger \cdot P_t - P_t^\dagger \cdot Q_t = 2iI, \quad (13)$$

where  $I$  is the  $D \times D$  identity matrix. Without any further approximation than the local harmonic approximation in Eq. (11), the solution of the time-dependent Schrödinger equation is equivalent to propagating the Gaussian's parameters as<sup>59,65,67</sup>

$$\dot{q}_t = m^{-1} \cdot p_t, \quad \dot{p}_t = -V'(q_t), \quad (14)$$

$$\dot{Q}_t = m^{-1} \cdot P_t, \quad \dot{P}_t = -V''(q_t) \cdot Q_t. \quad (15)$$

For Herzberg–Teller spectra,<sup>68</sup> where the transition dipole moment is a linear function of position, the initial wavepacket,

$$\phi(q, 0) = [\mu(q_0) + \mu'(q_0)^T \cdot (q - q_0)]\psi(q, 0), \quad (16)$$

is no longer a simple Gaussian. Nevertheless, such a wavepacket also preserves its form in the local harmonic potential (11),<sup>40–42</sup> namely

$$\phi(q, t) = [\mu(q_0) + \mu'(q_0)^T \cdot Q_0 \cdot Q_t^{-1} \cdot (q - q_t)]\psi(q, t), \quad (17)$$

where  $\psi(q, t)$  is the Gaussian wavepacket (10) propagated with the standard thawed Gaussian equations of motion for the parameters [Eqs. (14)–(15)]. This *extended* thawed Gaussian approximation has been recently applied to compute spectra beyond the Condon approximation.<sup>41,42</sup> In general, the Herzberg–Teller effect becomes important in weak or forbidden transitions, where the constant, Condon term of the transition dipole moment is small. However, it is hard to predict *a priori* whether this effect contributes to the spectrum.

The thawed Gaussian approximation requires not only potential energies and gradients but also Hessians at each point along the trajectory. This can become rather costly for accurate *ab initio* calculations of large molecules.<sup>36,60,69–80</sup> For this reason, two of us have proposed the *single-Hessian* thawed Gaussian approximation,<sup>39</sup> where  $V''(q_t)$  of Eq. (15) is replaced with the reference Hessian  $V''_{\text{ref}}(q_{\text{ref}})$  evaluated at a single (reference) point  $q_{\text{ref}}$ . The method was shown to perform well and consistently better than the standard global harmonic approaches in systems exhibiting moderate anharmonicity effects.<sup>39</sup> Moreover, it provides an estimate of the effect of anharmonicity on spectra at little additional computational cost: compared to the global harmonic method, it requires in addition only a single *ab initio* classical trajectory.

In Ref. 39, the single-Hessian thawed Gaussian approximation was used only for Gaussian wavepackets (10). Here, we combine the single-Hessian idea with the extended thawed Gaussian approximation in order to accelerate calculations of Herzberg–Teller spectra. Remarkably, Eq. (17) is unaffected with this change. In contrast, the conservation of energy, derived for the single-Hessian thawed Gaussian wavepacket in Ref. 39, does not hold in general for the extended thawed Gaussian wavepacket, for which the time derivative of the total energy is

$$\frac{dE}{dt} = \hbar \text{Re}[\mu(q_0)\mu'(q_0)^T \cdot Q_0 \cdot Q_t^\dagger \cdot b_t], \quad (18)$$

with  $b_t := (V''(q_t) - V''_{\text{ref}}(q_{\text{ref}})) \cdot m^{-1} \cdot p_t$  (see Supporting Information). Although the time derivative of energy (18) is non-zero in general, the energy is conserved in purely Herzberg–Teller spectra, i.e., if the constant, Condon, term  $\mu(q_0)$  is zero.

### 3 Computational and experimental details

To estimate adiabaticity with the MSDR, the underlying nuclear dynamics was based on Born-Oppenheimer dynamics, standard Tully’s fewest-switches surface hopping,<sup>43</sup> surface hopping with the energy-based decoherence correction,<sup>81</sup> or Ehrenfest dynamics. *Ab initio* trajectories were propagated using forces and NAC vectors obtained with CASSCF electronic structure. However, to simulate vibrationally resolved spectra, it is crucial to include dynamical correlation effects which are missing in CASSCF. To avoid cumbersome CASPT2 *ab initio* treatment, we employed the second-order algebraic diagrammatic construction [ADC(2)] method, which includes important correlation effects for a balanced treatment of so-called  $L_a$  and  $L_b$  states ( $S_2$  and  $S_1$  states in azulene, respectively).<sup>82</sup> A so-called “adiabatic Hessian”,<sup>39,53</sup> which is evaluated at the optimized geometry of the final electronic state, was used as the reference Hessian for the single-Hessian thawed Gaussian propagation. Dynamics and spectra simulations were performed with an in-house code coupled to Gaussian16,<sup>83</sup> Molpro2012,<sup>84,85</sup> and Molpro2015<sup>86,87</sup> electronic structure packages. For further details about dynamics simulations, electronic structure, and spectra computations, see Supporting Information.

The absorption spectra were recorded using a PerkinElmer Lambda 950 UV/Vis/NIR spectrophotometer in cyclohexane at room temperature with azulene concentration of  $10^{-5}$  M for  $S_2$  spectrum and  $10^{-3}$  M for the weaker  $S_1$  band. As for the emission, the spectra were recorded using a Horiba Jobin-Yvon Fluorolog-3 with a photomultiplier tube as a detector, the concentration was  $10^{-5}$  M in cyclohexane, and the sample was excited at 280 nm.

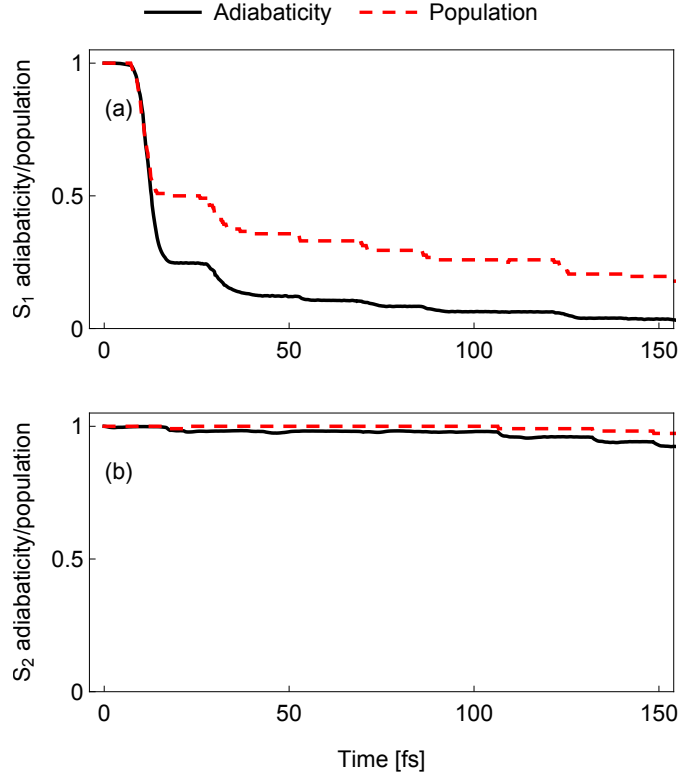


Figure 2: Adiabaticity [Eqs. (3)–(6)] and population decay for an ensemble of trajectories initiated at: a)  $S_1$  state or b)  $S_2$  state, and evolved with the fewest switches surface hopping algorithm<sup>43</sup> with decoherence correction.<sup>81</sup>

## 4 Results and discussion

### 4.1 Population dynamics and adiabaticity

Nonadiabatic dynamics, approximated with the decoherence-corrected surface hopping, was initiated in either the first or second excited state (Figure 2). Subsequent populations of  $S_1$  and  $S_2$  states illustrate well the violation of Kasha’s rule in azulene. On one hand, the system excited to  $S_1$  decays quickly to the ground state due to the accessible conical intersection seam. On the other hand, the system excited to  $S_2$  remains in that state, indicating that nonradiative decay is negligible. Interestingly, the  $S_1$  population decay appears as at least a biexponential process, where only the slower time constant is comparable to experiments.<sup>7</sup>

Despite the appealing picture provided by the population analysis, populations alone are

not sufficient to account for all non-Born-Oppenheimer effects, including the subtle effects of wavepacket displacement and interferences, including geometric phase, induced by NACs, even on a single potential energy surface.<sup>27,88</sup> Adiabaticity is, indeed, a more rigorous way to evaluate the importance of NACs. The MSDR, in turn, makes it possible to estimate adiabaticity with little additional computational cost. As shown in Fig. 2,  $S_1$  adiabaticity significantly drops already after 10 fs, which corresponds to the first arrival of the wavepacket to the conical intersection region, and gradually approaches zero within 150 fs. In the same time interval,  $S_2$  adiabaticity remains quite high. Overall, the computed adiabaticity provides additional support for the disparate behaviors of  $S_1$  and  $S_2$ . Interestingly, the  $S_1$  adiabaticity computed with the simple Born-Oppenheimer dynamics (see Fig. S2), which contains no information about populations whatsoever, resembles that of Fig. 2a. In contrast, mean-field Ehrenfest dynamics and standard surface hopping (without decoherence correction) yield higher adiabaticity of dynamics started from the  $S_1$  state and lower adiabaticity of dynamics started from  $S_2$ ; similar trends are observed for the initial-state populations (see Figs. S2–S5).

## 4.2 Absorption and emission spectra of azulene

Both population dynamics and adiabaticity suggest that the dynamics of a wavepacket initially in the  $S_2$  electronic state can be described rather well within the Born–Oppenheimer approximation, unlike the dynamics started in the  $S_1$  state, which exhibits fast nonradiative decay to the  $S_0$  ground state. Therefore, one would expect the thawed Gaussian approximation, a method that neglects nonadiabatic effects, to perform better for the  $S_2 \leftarrow S_0$  absorption spectrum than for the  $S_1 \leftarrow S_0$  absorption spectrum.

Surprisingly, the simulated  $S_1 \leftarrow S_0$  absorption spectrum (see Fig. 3a) agrees rather well with the experiment. It appears that, despite being considerably different from the true nonadiabatically evolved wavepacket, the thawed Gaussian wavepacket results in a correct autocorrelation function. Since only the part of the wavepacket that remains on the initial

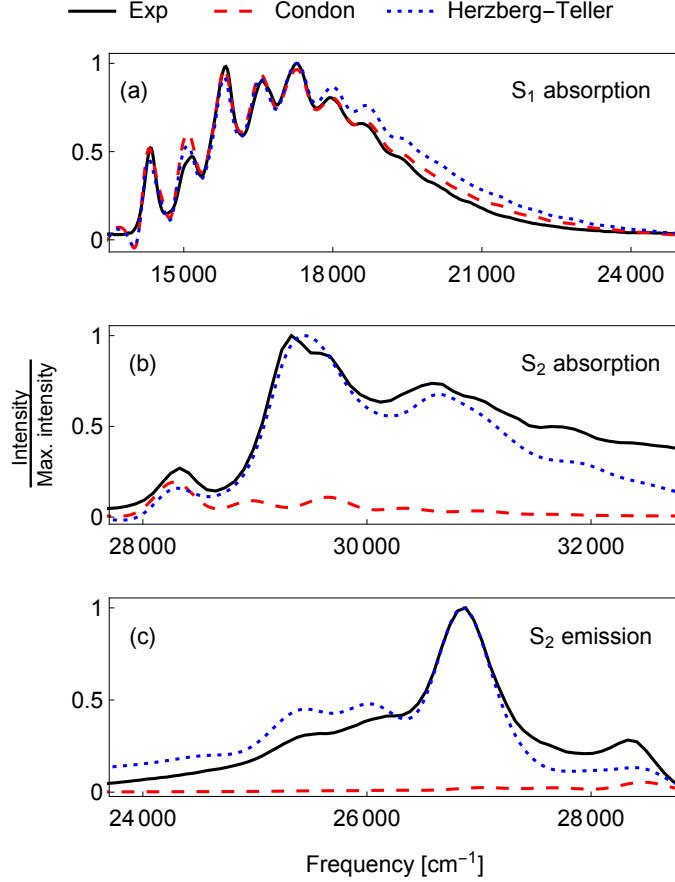


Figure 3: Vibrationally resolved (a)  $S_1 \leftarrow S_0$  absorption, (b)  $S_2 \leftarrow S_0$  absorption, and (c)  $S_2 \rightarrow S_0$  emission spectra of azulene. Calculations using adiabatic single-Hessian thawed Gaussian approximation (see Sec. 2.3 and Table S1) for the wavepacket dynamics and either Condon [ $\mu(q) \approx \mu(q_0)$ ] or Herzberg-Teller [Eq. (16)] approximations for the transition dipole moment are compared with the experiment. To facilitate this comparison, all computed spectra are shifted in frequency by a constant (see Table S2) and are rescaled to unit maximum intensity, except for those computed within the Condon approximation, which are scaled by the maxima of the corresponding Herzberg-Teller spectra.

state contributes to the autocorrelation function (8), a more convenient measure of nonadiabatic effects on spectra is obtained by dividing the adiabaticity by population. Adiabaticity is equal to the initial-state population when the nonadiabatic coupling affects only the amplitude but not the shape of the nuclear wavepacket on the initial surface. The ratio between the adiabaticity and initial-state population, shown in Fig. S6, decays less dramatically than the adiabaticity, which justifies partially the accuracy of the spectra computed using the Born–Oppenheimer wavepacket dynamics. In addition, rather short times are needed for the computation of the spectrum because it is only moderately resolved. One could expect the wavepacket autocorrelation function to exhibit increasingly more nonadiabatic effects at later times, implying that these effects would have to be included in the simulation of the high-resolution absorption spectrum. As already reported in Refs. 24 and 25, the  $S_1$  absorption spectrum can be computed easily within the Condon approximation and even using global harmonic models. Nevertheless, we observe an improvement of the computed spectrum by using the on-the-fly thawed Gaussian method that partially accounts for anharmonicity (see Fig. 4a); including the Herzberg–Teller contribution, however, does not improve the spectrum (Fig. 3a).

$S_2$  absorption and emission spectra are also well described by the single-Hessian extended thawed Gaussian approximation. The corresponding potential energy surface is harmonic in the regions visited by the nuclear wavepacket, which is confirmed by comparing spectra computed with thawed Gaussian and global harmonic approaches (see Figs. 4b and 4c). In contrast to the  $S_1$  spectrum, for describing the  $S_2$  spectra, the Herzberg–Teller contribution due to coupling with higher excited electronic states<sup>41,42,89</sup> is essential (see Figs. 3b and 3c). This effect has only been analyzed qualitatively in the emission spectrum of azulene, but never in the  $S_2$  absorption spectrum.<sup>15</sup>

Furthermore, the Herzberg–Teller coupling is responsible for the breakdown of mirror image symmetry between the absorption and emission spectra, which is formally valid only for a displaced harmonic oscillator model within the Condon approximation.<sup>90,91</sup> In general,

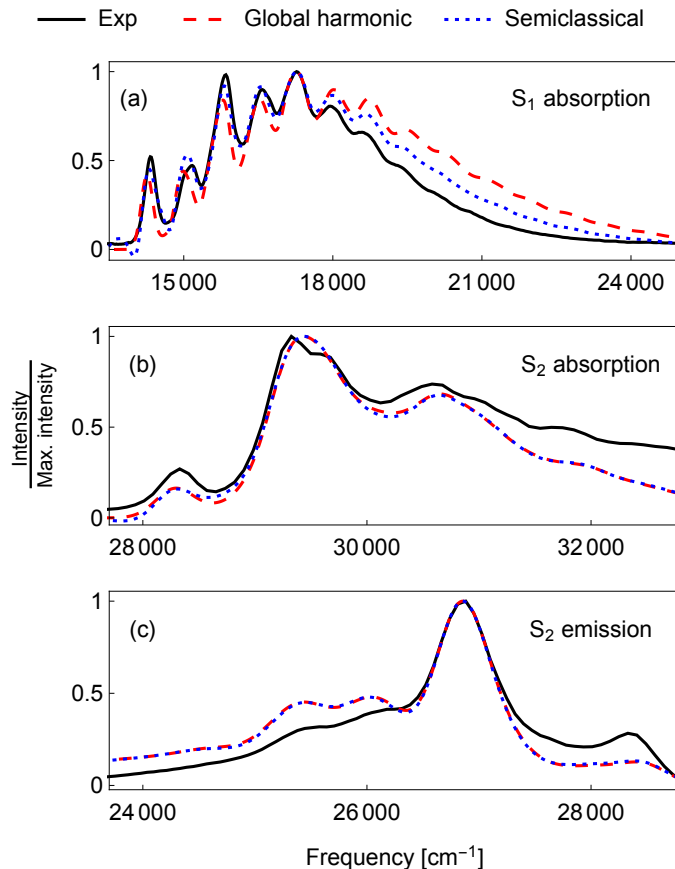


Figure 4: Vibrationally resolved (a)  $S_1 \leftarrow S_0$  absorption, (b)  $S_2 \leftarrow S_0$  absorption, and (c)  $S_2 \rightarrow S_0$  emission spectra of azulene. Calculations using adiabatic single-Hessian thawed Gaussian approximation (“semiclassical,” see Sec. 2.3 and Table S1) or adiabatic global harmonic approach (as described in Ref. 55)—both combined with the Herzberg–Teller approximation [Eq. (16)] for the transition dipole moment—are compared with the experiment. To facilitate this comparison, all computed spectra are rescaled to unit maximum intensity and shifted in frequency by a constant (see Table S2).



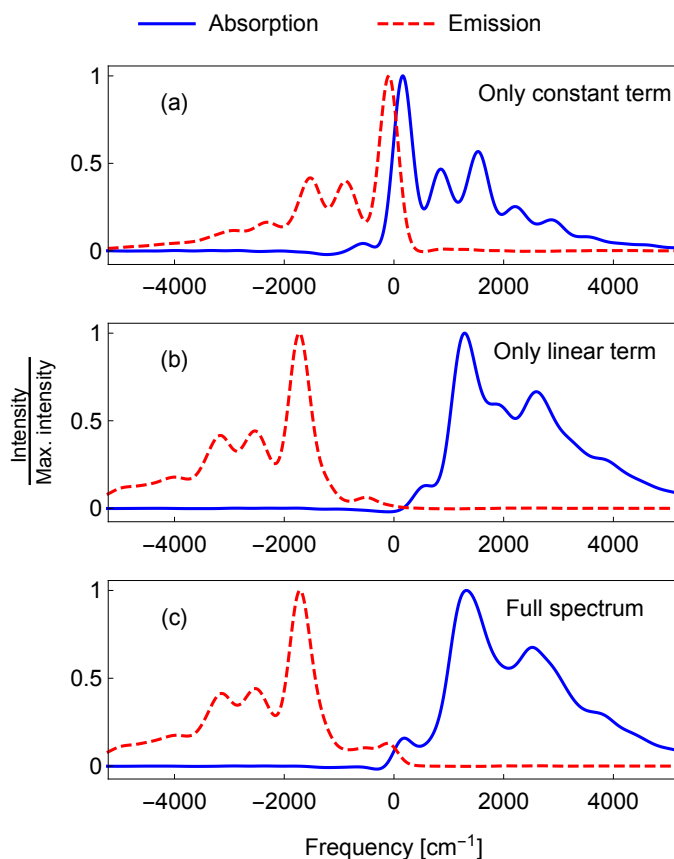


Figure 5: Vibrationally resolved  $S_2$  absorption and emission spectra of azulene computed with (a) only Condon (constant) term, (b) only Herzberg–Teller (linear) term, (c) both Condon and Herzberg–Teller terms in the expansion of the transition dipole moment [with all calculations using the adiabatic single-Hessian (extended) thawed Gaussian approximation (see Sec. 2.3 and Table S1)]. To facilitate comparison between absorption and emission, all spectra are rescaled to unit maximum intensity and shifted in frequency by a constant.

changes in the force constant, mode coupling, anharmonicity, and Herzberg–Teller coupling can all break this symmetry. In Fig. 5a, we show that the Condon absorption and emission spectra retain (to a large extent) this symmetry, whereas the mirror image symmetry is broken completely in the case of Herzberg–Teller spectra (see Fig. 5c). Such effect of the Herzberg–Teller coupling is well known,<sup>90,92–94</sup> but is commonly interpreted in terms of the cross terms that arise when both Condon and Herzberg–Teller contributions to the spectrum are significant. This is not the case here, as significant asymmetry is observed even for the pure Herzberg–Teller contribution (where the constant Condon term is set to zero, see Fig. 5b). In azulene, the breakdown of the mirror image symmetry between absorption and emission is a result of an interplay between the Herzberg–Teller and mode-mixing (Duschinsky) effects. Indeed, the symmetry is mostly recovered if either of the two effects is “turned off” (see Fig. 5a, where Herzberg–Teller coupling is set to zero, and Fig. S7, where mode mixing is neglected). More precisely, coupling between the modes modifies only slightly the dynamics of the Gaussian wavepacket, hence the similarity between the spectra in Figs. 5a and S7a, but affects considerably the linear, Herzberg–Teller term of the extended thawed Gaussian wavepacket (17), which explains the difference between the spectra in Figs. 5b and S7b. The Duschinsky effect on the absorption spectrum is largely due to couplings between the Herzberg–Teller active modes (see Fig. S8 where only those couplings are neglected). In contrast, the emission spectrum is only weakly affected by the mode-mode couplings (compare the emission spectra in Figs. 5c and S7c).

Small discrepancies between the simulated spectra and experiments are likely due to the accuracy of the electronic structure method. We found that the accuracy of the computed  $S_2 \leftarrow S_0$  absorption spectrum depends strongly on the degree of dynamic correlation included in the *ab initio* method (see Fig. S1). Accounting for finite-temperature and solvent effects, which are in our calculations included only phenomenologically through Gaussian broadening, might further improve the accuracy.<sup>54,95–101</sup>

## 5 Conclusion

To conclude, we presented a systematic and general semiclassical approach for studying photophysics beyond Kasha’s rule and spectroscopy beyond Condon’s approximation. We validated the method on the challenging case of azulene, where the proposed approach allowed us to consider the interplay of nonadiabatic, anharmonicity, mode-mixing, and Herzberg–Teller effects, as well as the importance of dynamical electron correlation in the electronic structure methods used. The presented methodology allows one to perform in-depth studies of photochemistry and photophysics of various molecular systems at a moderate computational cost.

## Acknowledgement

The authors acknowledge the financial support from the Swiss National Science Foundation through the NCCR MUST (Molecular Ultrafast Science and Technology) Network and from the European Research Council (ERC) under the European Union’s Horizon 2020 research and innovation programme (grant agreement No. 683069 – MOLEQULE).

## Supporting Information Available

The following files are available free of charge. Computational details, comparison of electronic structure methods for spectra calculations, energy conservation for the single-Hessian extended thawed Gaussian wavepacket, adiabaticity and population dynamics for different nuclear dynamics methods, adiabaticity divided by the initial-state population,  $S_2$  absorption and emission spectra simulated without Duschinsky mixing of the normal modes.

## References

- (1) Beer, M.; Longuet-Higgins, H. C. Anomalous light emission of azulene. *J. Chem. Phys.* **1955**, *23*, 1390–1391.
- (2) Viswanath, G.; Kasha, M. Confirmation of the Anomalous Fluorescence of Azulene. *J. Chem. Phys.* **1956**, *24*, 574–577.
- (3) McNaught, A. D., Wilkinson, A., Eds. *IUPAC. Compendium of Chemical Terminology, 2nd ed. (the "Gold Book")*; 1997; Online version (2019-) created by S. J. Chalk.
- (4) Ippen, E. P.; Shank, C. V.; Woerner, R. L. Picosecond dynamics of azulene. *Chem. Phys. Lett.* **1977**, *46*, 20–23.
- (5) Amirav, A.; Jortner, J. Spectroscopic manifestation of intramolecular relaxation of azulene in supersonic jets. *J. Chem. Phys.* **1984**, *81*, 4200–4205.
- (6) Huppert, D.; Jortner, J.; Rentzepis, P. M. S<sub>2</sub>-S<sub>1</sub> emission of azulene in solution. *Chem. Phys. Lett.* **1972**, *13*, 225–228.
- (7) Diau, E. W. G.; De Feyter, S.; Zewail, A. H. Direct observation of the femtosecond nonradiative dynamics of azulene in a molecular beam: The anomalous behavior in the isolated molecule. *J. Chem. Phys.* **1999**, *110*, 9785–9788.
- (8) Rentzepis, P. M. Emission from the lowest singlet and triplet states of azulene. *Chem. Phys. Lett.* **1969**, *3*, 717–720.
- (9) Foggi, P.; Neuwahl, F. V. R.; Moroni, L.; Salvi, P. R. S<sub>1</sub>-S<sub>n</sub> and S<sub>2</sub>-S<sub>n</sub> Absorption of Azulene: Femtosecond Transient Spectra and Excited State Calculations. *J. Phys. Chem. A* **2003**, *107*, 1689–1696.
- (10) Vosskötter, S.; Konieczny, P.; Marian, C. M.; Weinkauff, R. Towards an understanding of the singlet-triplet splittings in conjugated hydrocarbons: azulene investigated by

- anion photoelectron spectroscopy and theoretical calculations. *Phys. Chem. Chem. Phys.* **2015**, *17*, 23573–23581.
- (11) Gillispie, G. D.; Lim, E. C. Vibrational analysis of the S2-S1 fluorescence of azulene in a naphthalene mixed crystal at 4.2 K. *J. Chem. Phys.* **1978**, *68*, 4578–4586.
  - (12) Klemp, D.; Nickel, B. Phosphorescence and E-type delayed fluorescence from azulene in phenazine host crystals. *Chem. Phys.* **1983**, *78*, 17–28.
  - (13) Bearpark, M. J.; Bernardi, F.; Clifford, S.; Olivucci, M.; Robb, M. A.; Smith, B. R.; Vreven, T. The Azulene S1 State Decays via a Conical Intersection: A CASSCF Study with MMVB Dynamics. *J. Am. Chem. Soc.* **1996**, *118*, 169–175.
  - (14) Klein, S.; Bearpark, M. J.; Smith, B. R.; Robb, M. A.; Olivucci, M.; Bernardi, F. Mixed state 'on the fly' non-adiabatic dynamics: The role of the conical intersection topology. *Chem. Phys. Lett.* **1998**, *292*, 259–266.
  - (15) Gustav, K.; Storch, M. Vibronic spectral behavior of molecules. XIII. Theoretical contribution to the vibronic coupling and the dushinsky effect on the S1-S0 absorption and the S1-S0, S2-S1, and S2-S0 fluorescences of azulene. *Int. J. Quant. Chem.* **1990**, *38*, 25–39.
  - (16) Negri, F.; Zgierski, M. Z. On the vibronic structure of the S0 $\leftrightarrow$ S1 transitions in azulene. *J. Chem. Phys.* **1993**, *99*, 4318–4326.
  - (17) Amatatsu, Y.; Komura, Y. Reaction coordinate analysis of the S1-S0 internal conversion of azulene. *J. Chem. Phys.* **2006**, *125*, 174311.
  - (18) Murakami, A.; Kobayashi, T.; Goldberg, A.; Nakamura, S. CASSCF and CASPT2 studies on the structures, transition energies, and dipole moments of ground and excited states for azulene. *J. Chem. Phys.* **2004**, *120*, 1245–1252.

- (19) Del Valle, J. C.; Catalán, J. Kasha’s rule: A reappraisal. *Phys. Chem. Chem. Phys.* **2019**, *21*, 10061–10069.
- (20) Paul, L.; Moitra, T.; Ruud, K.; Chakrabarti, S. Strong Duschinsky Mixing Induced Breakdown of Kasha’s Rule in an Organic Phosphor. *J. Phys. Chem. Lett.* **2019**, *10*, 369–374.
- (21) Röhrs, M.; Escudero, D. Multiple Anti-Kasha Emissions in Transition-Metal Complexes. *J. Phys. Chem. Lett.* **2019**, *10*, 5798–5804.
- (22) Shafikov, M. Z.; Brandl, F.; Dick, B.; Czerwieniec, R. Can Coumarins Break Kasha’s Rule? *J. Phys. Chem. Lett.* **2019**, *10*, 6468–6471.
- (23) Zhou, P.; Li, P.; Zhao, Y.; Han, K. Restriction of Flip-flop Motion as a Mechanism for Aggregation-Induced Emission. *J. Phys. Chem. Lett.* **2019**, *10*, 6929–6935.
- (24) Dierksen, M.; Grimme, S. Density functional calculations of the vibronic structure of electronic absorption spectra. *J. Chem. Phys.* **2004**, *120*, 3544–3554.
- (25) Niu, Y.; Peng, Q.; Deng, C.; Gao, X.; Shuai, Z. Theory of excited state decays and optical spectra: Application to polyatomic molecules. *J. Phys. Chem. A* **2010**, *114*, 7817–7831.
- (26) Condon, E. U. Nuclear motions associated with electron transitions in diatomic molecules. *Phys. Rev.* **1928**, *32*, 858 – 872.
- (27) Zimmermann, T.; Vaníček, J. Measuring nonadiabaticity of molecular quantum dynamics with quantum fidelity and with its efficient semiclassical approximation. *J. Chem. Phys.* **2012**, *136*, 094106.
- (28) Zimmermann, T.; Vaníček, J. Evaluation of the importance of spin-orbit couplings in the nonadiabatic quantum dynamics with quantum fidelity and with its efficient ”on-the-fly” ab initio semiclassical approximation. *J. Chem. Phys.* **2012**, *137*, 22A516.

- (29) Martens, C. C.; Fang, J. Y. Semiclassical-limit molecular dynamics on multiple electronic surfaces. *J. Chem. Phys.* **1997**, *106*, 4918–4930.
- (30) Müller, U.; Stock, G. Surface-hopping modeling of photoinduced relaxation dynamics on coupled potential-energy surfaces. *J. Chem. Phys.* **1997**, *107*, 6230–6245.
- (31) Worth, G. A.; Hunt, P.; Robb, M. A. Nonadiabatic dynamics: A comparison of surface hopping direct dynamics with quantum wavepacket calculations. *J. Phys. Chem. A* **2003**, *107*, 621–631.
- (32) Tapavicza, E.; Tavernelli, I.; Rothlisberger, U.; Filippi, C.; Casida, M. E. Mixed time-dependent density-functional theory/classical trajectory surface hopping study of oxirane photochemistry. *J. Chem. Phys.* **2008**, *129*.
- (33) Richter, M.; Marquetand, P.; González-Vázquez, J.; Sola, I.; González, L. SHARC: Ab initio molecular dynamics with surface hopping in the adiabatic representation including arbitrary couplings. *J. Chem. Theory Comput.* **2011**, *7*, 1253–1258.
- (34) Curchod, B. F. E.; Tavernelli, I.; Rothlisberger, U. Trajectory-based solution of the nonadiabatic quantum dynamics equations: An on-the-fly approach for molecular dynamics simulations. *Phys. Chem. Chem. Phys.* **2011**, *13*, 3231–3236.
- (35) Belyaev, A. K.; Lasser, C.; Trigila, G. Landau-Zener type surface hopping algorithms. *J. Chem. Phys.* **2014**, *140*, 224108.
- (36) Richings, G. W.; Polyak, I.; Spinlove, K. E.; Worth, G. A.; Burghardt, I.; Lasorne, B. Quantum Dynamics Simulations Using Gaussian Wavepackets: the vMCG Method. *Int. Rev. Phys. Chem.* **2015**, *34*, 269–308.
- (37) Curchod, B. F. E.; Agostini, F.; Tavernelli, I. CT-MQC a coupled-trajectory mixed quantum/classical method including nonadiabatic quantum coherence effects. *Eur. Phys. J. B* **2018**, *91*, 168.

- (38) Glover, W. J.; Mori, T.; Schuurman, M. S.; Boguslavskiy, A. E.; Schalk, O.; Stolow, A.; Martínez, T. J. Excited state non-adiabatic dynamics of the smallest polyene, trans 1,3-butadiene. II. Ab initio multiple spawning simulations. *J. Chem. Phys.* **2018**, *148*, 164303.
- (39) Begušić, T.; Cordova, M.; Vaníček, J. Single-Hessian thawed Gaussian approximation. *J. Chem. Phys.* **2019**, *150*, 154117.
- (40) Lee, S.-Y.; Heller, E. J. Exact time-dependent wave packet propagation: Application to the photodissociation of methyl iodide. *J. Chem. Phys.* **1982**, *76*, 3035–3044.
- (41) Patoz, A.; Begušić, T.; Vaníček, J. On-the-Fly Ab Initio Semiclassical Evaluation of Absorption Spectra of Polyatomic Molecules beyond the Condon Approximation. *J. Phys. Chem. Lett.* **2018**, *9*, 2367–2372.
- (42) Begušić, T.; Patoz, A.; Šulc, M.; Vaníček, J. On-the-fly ab initio three thawed Gaussians approximation: a semiclassical approach to Herzberg-Teller spectra. *Chem. Phys.* **2018**, *515*, 152–163.
- (43) Tully, J. C. Molecular dynamics with electronic transitions. *J. Chem. Phys.* **1990**, *93*, 1061–1071.
- (44) Crespo-Otero, R.; Barbatti, M. Recent Advances and Perspectives on Nonadiabatic Mixed QuantumClassical Dynamics. *Chem. Rev.* **2018**, *118*, 7026–7068.
- (45) Zimmermann, T.; Vaníček, J. Communications: Evaluation of the nondiabaticity of quantum molecular dynamics with the dephasing representation of quantum fidelity. *J. Chem. Phys.* **2010**, *132*, 241101.
- (46) MacKenzie, R.; Pineault, M.; Renaud-Desjardins, L. Optimizing adiabaticity in quantum mechanics. *Can. J. Phys.* **2012**, *90*, 187.



- (47) Vaníček, J. Several Semiclassical Approaches to Time-resolved Spectroscopy. *CHIMIA* **2017**, *71*, 283–287.
- (48) Heller, E. J. The semiclassical way to molecular spectroscopy. *Acc. Chem. Res.* **1981**, *14*, 368–375.
- (49) Tannor, D. J. *Introduction to Quantum Mechanics: A Time-Dependent Perspective*; University Science Books: Sausalito, 2007.
- (50) Lami, A.; Petrongolo, C.; Santoro, F. In *Conical intersections: Electronic structure, dynamics and spectroscopy*; Domcke, W., Yarkony, D. R., Köppel, H., Eds.; World Scientific Publishing: Singapore, 2004; Chapter 16, pp 699–738.
- (51) Craig, D. P.; Thirunamachandran, T. *Molecular Quantum Electrodynamics*; Academic Press Inc.: Orlando, 1984.
- (52) Santoro, F.; Imbrota, R.; Lami, A.; Bloino, J.; Barone, V. Effective method to compute Franck-Condon integrals for optical spectra of large molecules in solution. *J. Chem. Phys.* **2007**, *126*, 084509.
- (53) Avila Ferrer, F. J.; Santoro, F. Comparison of vertical and adiabatic harmonic approaches for the calculation of the vibrational structure of electronic spectra. *Phys. Chem. Chem. Phys.* **2012**, *14*, 13549–13563.
- (54) Baiardi, A.; Bloino, J.; Barone, V. General Time Dependent Approach to Vibronic Spectroscopy Including Franck-Condon, Herzberg-Teller, and Duschinsky Effects. *J. Chem. Theory Comput.* **2013**, *9*, 4097–4115.
- (55) Santoro, F.; Jacquemin, D. Going beyond the vertical approximation with time-dependent density functional theory. *WIREs Comput. Mol. Sci.* **2016**, *6*, 460–486.

- (56) Benkyi, I.; Tapavicza, E.; Fliegl, H.; Sundholm, D. Calculation of vibrationally resolved absorption spectra of acenes and pyrene. *Phys. Chem. Chem. Phys.* **2019**, *21*, 21094–21103.
- (57) Tapavicza, E. Generating Function Approach to Single Vibronic Level Fluorescence Spectra. *J. Phys. Chem. Lett.* **2019**, *10*, 6003–6009.
- (58) Zimmermann, T.; Vaníček, J. Efficient on-the-fly ab initio semiclassical method for computing time-resolved nonadiabatic electronic spectra with surface hopping or Ehrenfest dynamics. *J. Chem. Phys.* **2014**, *141*.
- (59) Heller, E. J. Time-dependent approach to semiclassical dynamics. *J. Chem. Phys.* **1975**, *62*, 1544–1555.
- (60) Wehrle, M.; Šulc, M.; Vaníček, J. On-the-fly Ab Initio Semiclassical Dynamics: Identifying Degrees of Freedom Essential for Emission Spectra of Oligothiophenes. *J. Chem. Phys.* **2014**, *140*, 244114.
- (61) Wehrle, M.; Oberli, S.; Vaníček, J. On-the-fly ab initio semiclassical dynamics of floppy molecules: Absorption and photoelectron spectra of ammonia. *J. Phys. Chem. A* **2015**, *119*, 5685.
- (62) Heller, E. J. Classical S-matrix limit of wave packet dynamics. *J. Chem. Phys.* **1976**, *65*, 4979–4989.
- (63) Hagedorn, G. A. Semiclassical quantum mechanics. I. The  $\hbar \rightarrow 0$  limit for coherent states. *Commun. Math. Phys.* **1980**, *71*, 77–93.
- (64) Hagedorn, G. A. Raising and Lowering Operators for Semiclassical Wave Packets. *Ann. Phys. (NY)* **1998**, *269*, 77–104.
- (65) Faou, E.; Gradinaru, V.; Lubich, C. Computing semiclassical quantum dynamics with Hagedorn wavepackets. *SIAM J. Sci. Comput.* **2009**, *31*, 3027–3041.

- (66) Note that the right-hand side of Eq. 13 can take different constant values, depending on the choice of initial  $Q_0$  and  $P_0$ ; these can be chosen arbitrarily, as long as the product  $P_0 \cdot Q_0^{-1}$  is conserved. The value  $2iI$  is obtained for  $Q_0 = \text{Im}(P_0 \cdot Q_0^{-1})^{-1/2}$  and follows the notation of Ref. 65. The reader is referred to Appendix B of Ref. 39 for further details.
- (67) Lubich, C. *From Quantum to Classical Molecular Dynamics: Reduced Models and Numerical Analysis*, 12th ed.; European Mathematical Society: Zürich, 2008.
- (68) Herzberg, G.; Teller, E. Schwingungsstruktur der Elektronenübergänge Bei Mehratomigen Molekülen. *Z. Phys. Chem. B* **1933**, *21*, 410.
- (69) Tatchen, J.; Pollak, E. Semiclassical on-the-fly computation of the  $S_0 \rightarrow S_1$  absorption spectrum of formaldehyde. *J. Chem. Phys.* **2009**, *130*, 041103.
- (70) Ceotto, M.; Zhuang, Y.; Hase, W. L. Accelerated direct semiclassical molecular dynamics using a compact finite difference Hessian scheme. *J. Chem. Phys.* **2013**, *138*, 054116.
- (71) Zhuang, Y.; Siebert, M. R.; Hase, W. L.; Kay, K. G.; Ceotto, M. Evaluating the accuracy of Hessian approximations for direct dynamics simulations. *J. Chem. Theory Comput.* **2013**, *9*, 54–64.
- (72) Ianconescu, R.; Tatchen, J.; Pollak, E. On-the-fly Semiclassical Study of Internal Conversion Rates of Formaldehyde. *J. Chem. Phys.* **2013**, *139*, 154311.
- (73) Richings, G. W.; Worth, G. A. A Practical Diabatisation Scheme for Use with the Direct-Dynamics Variational Multi-Configuration Gaussian Method. *J. Phys. Chem. A* **2015**, *119*, 12457–12470.
- (74) Alborzpour, J. P.; Tew, D. P.; Habershon, S. Efficient and accurate evaluation of

- potential energy matrix elements for quantum dynamics using Gaussian process regression. *J. Chem. Phys.* **2016**, *145*, 174112.
- (75) Laude, G.; Calderini, D.; Tew, D. P.; Richardson, J. O. Ab initio instanton rate theory made efficient using Gaussian process regression. *Faraday Discuss.* **2018**, *212*, 237–258.
- (76) Bonfanti, M.; Petersen, J.; Eisenbrandt, P.; Burghardt, I.; Pollak, E. Computation of the S1 S0 vibronic absorption spectrum of formaldehyde by variational Gaussian wavepacket and semiclassical IVR methods. *J. Chem. Theory Comput.* **2018**, *14*, 5310–4323.
- (77) Polyak, I.; Richings, G. W.; Habershon, S.; Knowles, P. J. Direct quantum dynamics using variational Gaussian wavepackets and Gaussian process regression. *J. Chem. Phys.* **2019**, *150*, 041101.
- (78) Conte, R.; Gabas, F.; Botti, G.; Zhuang, Y.; Ceotto, M. Semiclassical vibrational spectroscopy with Hessian databases. *J. Chem. Phys.* **2019**, *150*, 244118.
- (79) Gabas, F.; Di Liberto, G.; Ceotto, M. Vibrational investigation of nucleobases by means of divide and conquer semiclassical dynamics. *J. Chem. Phys.* **2019**, *150*, 184113.
- (80) Micciarelli, M.; Gabas, F.; Conte, R.; Ceotto, M. An effective semiclassical approach to IR spectroscopy. *J. Chem. Phys.* **2019**, *150*, 184113.
- (81) Granucci, G.; Persico, M. Critical appraisal of the fewest switches algorithm for surface hopping. *J. Chem. Phys.* **2007**, *126*, 134114.
- (82) Prlj, A.; Sandoval-Salinas, M. E.; Casanova, D.; Jacquemin, D.; Corminboeuf, C. Low-Lying  $\pi\pi^*$  States of Heteroaromatic Molecules: A Challenge for Excited State Methods. *J. Chem. Theory Comput.* **2016**, *12*, 2652–2660.

- (83) Frisch, M. J.; Trucks, G. W.; Schlegel, H. B.; Scuseria, G. E.; Robb, M. A.; Cheeseman, J. R.; Scalmani, G.; Barone, V.; Petersson, G. A.; Nakatsuji, H.; Li, X.; Caricato, M.; Marenich, A. V.; Bloino, J.; Janesko, B. G.; Gomperts, R.; Men-  
nucci, B.; Hratchian, H. P.; Ortiz, J. V.; Izmaylov, A. F.; Sonnenberg, J. L.; Williams-  
Young, D.; Ding, F.; Lipparini, F.; Egidi, F.; Goings, J.; Peng, B.; Petrone, A.;  
Henderson, T.; Ranasinghe, D.; Zakrzewski, V. G.; Gao, J.; Rega, N.; Zheng, G.;  
Liang, W.; Hada, M.; Ehara, M.; Toyota, K.; Fukuda, R.; Hasegawa, J.; Ishida, M.;  
Nakajima, T.; Honda, Y.; Kitao, O.; Nakai, H.; Vreven, T.; Throssell, K.; Mont-  
gomery, J. A., Jr.; Peralta, J. E.; Ogliaro, F.; Bearpark, M. J.; Heyd, J. J.; Broth-  
ers, E. N.; Kudin, K. N.; Staroverov, V. N.; Keith, T. A.; Kobayashi, R.; Normand, J.;  
Raghavachari, K.; Rendell, A. P.; Burant, J. C.; Iyengar, S. S.; Tomasi, J.; Cossi, M.;  
Millam, J. M.; Klene, M.; Adamo, C.; Cammi, R.; Ochterski, J. W.; Martin, R. L.;  
Morokuma, K.; Farkas, O.; Foresman, J. B.; Fox, D. J. Gaussian 16 Revision C.01.  
2016; Gaussian Inc. Wallingford CT.
- (84) Werner, H.-J.; Knowles, P. J.; Knizia, G.; Manby, F. R.; Schütz, M. Molpro: a general-  
purpose quantum chemistry program package. *WIREs Comput. Mol. Sci.* **2012**, *2*,  
242–253.
- (85) Werner, H.-J.; Knowles, P. J.; Knizia, G.; Manby, F. R.; Schütz, M.; Celani, P.; Ko-  
rona, T.; Lindh, R.; Mitrushenkov, A.; Rauhut, G.; Shamasundar, K. R.; Adler, T. B.;  
Amos, R. D.; Bernhardsson, A.; Berning, A.; Cooper, D. L.; Deegan, M. J. O.; Dob-  
byn, A. J.; Eckert, F.; Goll, E.; Hampel, C.; Hesselmann, A.; Hetzer, G.; Hrenar, T.;  
Jansen, G.; Köppl, C.; Liu, Y.; Lloyd, A. W.; Mata, R. A.; May, A. J.; McNi-  
cholas, S. J.; Meyer, W.; Mura, M. E.; Nicklass, A.; O’Neill, D. P.; Palmieri, P.;  
Peng, D.; Pflüger, K.; Pitzer, R.; Reiher, M.; Shiozaki, T.; Stoll, H.; Stone, A. J.;  
Tarroni, R.; Thorsteinsson, T.; Wang, M. MOLPRO, version 2012.1, a package of ab  
initio programs. 2012; see <http://www.molpro.net>.

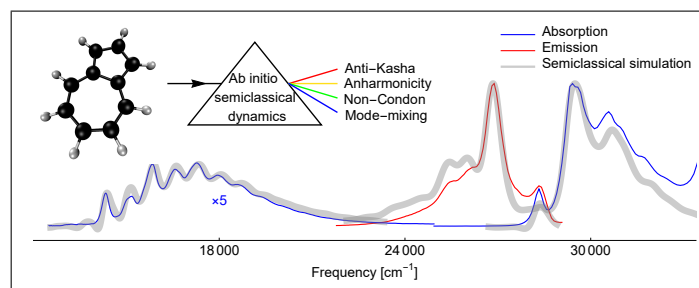
- (86) Werner, H.-J.; Knowles, P. J.; Knizia, G.; Manby, F. R.; Schütz, M.; Celani, P.; Györffy, W.; Kats, D.; Korona, T.; Lindh, R.; Mitrushenkov, A.; Rauhut, G.; Shamasundar, K. R.; Adler, T. B.; Amos, R. D.; Bernhardsson, A.; Berning, A.; Cooper, D. L.; Deegan, M. J. O.; Dobbyn, A. J.; Eckert, F.; Goll, E.; Hampel, C.; Hesselmann, A.; Hetzer, G.; Hrenar, T.; Jansen, G.; Köppl, C.; Liu, Y.; Lloyd, A. W.; Mata, R. A.; May, A. J.; McNicholas, S. J.; Meyer, W.; Mura, M. E.; Nicklass, A.; O'Neill, D. P.; Palmieri, P.; Peng, D.; Pflüger, K.; Pitzer, R.; Reiher, M.; Shiozaki, T.; Stoll, H.; Stone, A. J.; Tarroni, R.; Thorsteinsson, T.; Wang, M. MOLPRO, version 2015.1, a package of ab initio programs. 2015; see "<http://www.molpro.net>".
- (87) Kats, D.; Schütz, M. A multistate local coupled cluster CC2 response method based on the Laplace transform. *J. Chem. Phys.* **2009**, *131*, 124117.
- (88) Xie, C.; Malbon, C. L.; Guo, H.; Yarkony, D. R. Up to a Sign. The Insidious Effects of Energetically Inaccessible Conical Intersections on Unimolecular Reactions. *Acc. Chem. Res.* **2019**, *52*, 501–509.
- (89) Li, J.; Lin, C.-K.; Li, X. Y.; Zhu, C. Y.; Lin, S. H. Symmetry Forbidden Vibronic Spectra and Internal Conversion in Benzene. *Phys. Chem. Chem. Phys.* **2010**, *12*, 14967–76.
- (90) Santoro, F.; Lami, A.; Improta, R.; Bloino, J.; Barone, V. Effective method for the computation of optical spectra of large molecules at finite temperature including the Duschinsky and Herzberg-Teller effect: The Qx band of porphyrin as a case study. *J. Chem. Phys.* **2008**, *128*, 224311.
- (91) Galestian Pour, A.; Lincoln, C. N.; Perlík, V.; Šanda, F.; Hauer, J. Anharmonic vibrational effects in linear and two-dimensional electronic spectra. *Phys. Chem. Chem. Phys.* **2017**, *19*, 24752–24760.
- (92) Geigle, K. P.; Wolf, J.; Hohlneicher, G. Franck-Condon/Herzberg-Teller interferences

- in the 1Lb transitions of pyrene and chrysene. *J. Photochem. Photobiol. A-Chem.* **1997**, *105*, 183–187.
- (93) Toutounji, M. Linear and nonlinear Herzberg-Teller vibronic coupling effects. I: Electronic photon echo spectroscopy. *Chem. Phys.* **2019**, *521*, 25–34.
- (94) Toutounji, M. A deeper look into Herzberg-Teller vibronic coupling effect and spectroscopic signature of non-Condon systems. *Chem. Phys.* **2019**, *523*, 205–210.
- (95) Reddy, C. S.; Prasad, M. D. A Gaussian Wave Packet Propagation Approach to Vibrationally Resolved Optical Spectra at Non-Zero Temperatures. *J. Phys. Chem. A* **2016**, *120*, 2583–2590.
- (96) Borrelli, R.; Gelin, M. F. Quantum electron-vibrational dynamics at finite temperature: Thermo field dynamics approach. *J. Chem. Phys.* **2016**, *145*, 224101.
- (97) Chen, L.; Zhao, Y. Finite temperature dynamics of a Holstein polaron: The thermo-field dynamics approach. *J. Chem. Phys.* **2017**, *147*, 214102.
- (98) Chen, L.; Zhao, Y.; Tanimura, Y. Dynamics of a One-Dimensional Holstein Polaron with the Hierarchical Equations of Motion Approach. *J. Phys. Chem. Lett.* **2015**, *6*, 3110–3115.
- (99) Loco, D.; Jurinovich, S.; Cupellini, L.; Menger, M. F. S. J.; Mennucci, B. The modeling of the absorption lineshape for embedded molecules through a polarizable QM/MM approach. *Photochem. Photobiol. Sci.* **2018**, *17*, 552–560.
- (100) Loco, D.; Cupellini, L. Modeling the absorption lineshape of embedded systems from molecular dynamics: A tutorial review. *Int. J. Quant. Chem.* **2019**, *119*, 1–14.
- (101) Fortino, M.; Bloino, J.; Collini, E.; Bolzonello, L.; Trapani, M.; Faglioni, F.; Pedone, A. On the simulation of vibrationally resolved electronic spectra of medium-size

molecules: the case of styryl substituted BODIPYs. *Phys. Chem. Chem. Phys.* **2019**, 5–15.



# Graphical TOC Entry



**Supporting information for:**

**Semiclassical Approach to Photophysics Beyond  
Kasha's Rule and Vibronic Spectroscopy Beyond  
the Condon Approximation. The Case of Azulene**

Antonio Prlj,<sup>†,¶</sup> Tomislav Begušić,<sup>†,¶</sup> Zhan Tong Zhang,<sup>†</sup> George Cameron  
Fish,<sup>‡</sup> Marius Wehrle,<sup>†</sup> Tomáš Zimmermann,<sup>†</sup> Seonghoon Choi,<sup>†</sup> Julien Roulet,<sup>†</sup>  
Jacques-Edouard Moser,<sup>\*,‡</sup> and Jiří Vaníček<sup>\*,†</sup>

<sup>†</sup>*Laboratory of Theoretical Physical Chemistry, Institut des Sciences et Ingénierie  
Chimiques, Ecole Polytechnique Fédérale de Lausanne (EPFL), CH-1015, Lausanne,  
Switzerland*

<sup>‡</sup>*Photochemical Dynamics Group, Institut des Sciences et Ingénierie Chimiques, Ecole  
Polytechnique Fédérale de Lausanne (EPFL), CH-1015, Lausanne, Switzerland*

<sup>¶</sup>*These authors contributed equally.*

## Computational details

Minima of  $S_0$ ,  $S_1$ , and  $S_2$  states, as well as minimum energy conical intersection between  $S_0$  and  $S_1$  were optimized at SA5-CASSCF(4,6)/6-31G\* level. To compute the potential energy surface cuts in Fig. 1, we performed linear interpolation of internal coordinates between the optimized geometries, while the section of the surface beyond the  $S_2$  minimum was based on internal coordinate extrapolation. All dynamics simulations were performed for 800 time steps of 8 a.u. (0.1935 fs) each, therefore, for the total time of  $\approx 155$  fs. The velocity Verlet algorithm was used to integrate classical equations of motion.

## Multiple-surface dephasing representation (MSDR)

Ensembles of  $N = 112$  *ab initio* trajectories were propagated with each nuclear dynamics method (i.e., Born-Oppenheimer, fewest-switches surface hopping, or Ehrenfest dynamics). Note that by “Ehrenfest dynamics” we mean a locally mean field dynamics,<sup>S1</sup> i.e., an independent Ehrenfest dynamics of each trajectory in the ensemble. For nonadiabatic dynamics, ground and four excited states were taken into account. Energies, gradients, and nonadiabatic couplings were computed with state-averaged complete active space self-consistent field [SA5-CASSCF(4,6)/6-31G\*] electronic structure method, as implemented in Molpro2012.<sup>S2,S3</sup> Compared to CASSCF with larger active spaces [(6,6),(10,10)], which give an incorrect ground state minimum structure with  $C_s$  symmetry, CASSCF(4,6) has a correct  $C_{2v}$  minimum. Initial positions and momenta were sampled from the Wigner distribution of a vibrational ground state of a harmonic fit to the ground potential energy surface. Assuming the vertical excitation, the whole ensemble of trajectories was launched from either the  $S_1$  or  $S_2$  state. Surface hopping simulations were performed both without<sup>S4</sup> and with an energy-based decoherence correction,<sup>S5</sup> which was applied at every nuclear time step, with a parameter  $\alpha = 0.1$  Hartree.

# On-the-fly *ab initio* thawed Gaussian propagation and spectra

For computing vibronic spectra, three electronic structure methods were tested: (i) (time-dependent) density functional theory (in combination with the B3LYP functional and TZVP basis set, which were used in Ref. S6); (ii) SA5-CASSCF(4,6)/6-31G\* (used also for MSDR calculations); (iii) second-order Møller–Plesset perturbation theory (MP2) for ground state combined with the second-order algebraic diagrammatic construction [ADC(2)] scheme for the excited states (cc-pVDZ basis set). Gaussian 16 package<sup>S7</sup> was used for (time-dependent) density functional theory calculations, while Molpro2015<sup>S8</sup> was used for CASSCF, MP2, and ADC(2) methods. For ADC(2) calculations, we used Laplace transformed density-fitted local ADC(2) implementation in Molpro [keyword LT-DF-LADC(2)].<sup>S9</sup> Spectra computed with these electronic structure methods—including the Herzberg–Teller term of the transition dipole moment, but only within the adiabatic global harmonic approximation for the potential energy—are compared in Fig. S1.

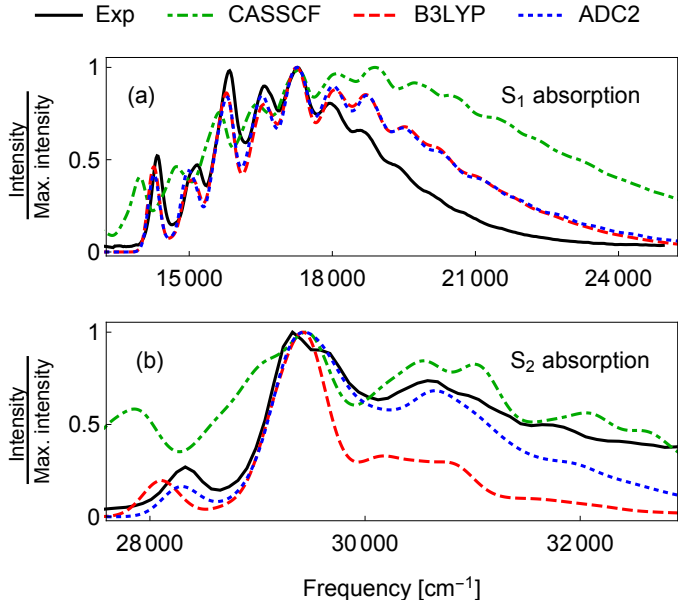


Figure S1:  $S_1 \leftarrow S_0$  and  $S_2 \leftarrow S_0$  absorption spectra computed using different electronic structure methods.

The trajectories needed for evaluating the  $S_1 \leftarrow S_0$  and  $S_2 \leftarrow S_0$  absorption spectra with the single-Hessian extended thawed Gaussian approximation were propagated with the

excited-state ADC(2) gradients, starting from the ground-state geometry optimized at the MP2 level. Similarly, the trajectory needed for computing the  $S_2 \rightarrow S_0$  emission spectrum started at the  $S_2$  minimum [found by geometry optimization at the ADC(2) level of theory] and was run using MP2 gradients of the ground-state potential energy surface. In all cases, the initial wavepacket was the ground vibrational state of the harmonic potential fit to the potential energy surface of the initial electronic state. Gaussian wavepacket propagation was performed in normal-mode coordinates obtained by diagonalizing the mass-scaled initial-state Hessian, so that the initial wavepacket was a simple product of one-dimensional Gaussian functions. For each single-Hessian thawed Gaussian propagation, the reference Hessian was chosen as the adiabatic Hessian of the final electronic state (see Table S1).

Table S1: Parameters used in the calculations of various spectra with the adiabatic single-Hessian extended thawed Gaussian approximation.

	$S_1$ absorption	$S_2$ absorption	$S_2$ emission
Initial geometry $q_0$	$q_{\text{eq}}(S_0)$	$q_{\text{eq}}(S_0)$	$q_{\text{eq}}(S_2)$
Reference Hessian $V''_{\text{ref}}$	$V''_{S_1}$	$V''_{S_2}$	$V''_{S_0}$
Reference geometry $q_{\text{ref}}$	$q_{\text{eq}}(S_1)$	$q_{\text{eq}}(S_2)$	$q_{\text{eq}}(S_0)$

Derivatives of the electronic transition dipole moment with respect to nuclear coordinates are not readily available in quantum chemistry packages. We evaluated them by finite differences, i.e., by computing the transition dipole moments at geometries displaced by 0.01 a.u. from the optimized initial-state geometry. Fortunately, these numbers can be extracted from the output of the *ab initio* numerical excited-state force or Hessian calculation.<sup>S10–S12</sup>

Spectral broadening was introduced by multiplying the autocorrelation function with a Gaussian damping function, which is equivalent to convolving the spectrum with another, but related Gaussian function. To facilitate the comparison between computed and experimental spectra, we introduced a constant energy shift in each spectrum. Because the constant shift error arises mostly due to the incorrect *ab initio* vertical energy gap, the same shifts were applied to Condon and Herzberg–Teller spectra. Broadening and energy shift parameters are given in Table S2.

Table S2: Half-width at half-maximum (HWHM) of the Gaussian broadening functions and horizontal energy shifts applied to spectra computed with global harmonic models or thawed Gaussian approximation (TGA). All values are expressed in  $\text{cm}^{-1}$ . Exceptionally, in Fig. 5 of the main text and Fig. S7, HWHM was  $200 \text{ cm}^{-1}$  for both  $\text{S}_2$  absorption and emission spectra.

	$\text{S}_1$ absorption	$\text{S}_2$ absorption	$\text{S}_2$ emission
HWHM	140	200	250
Energy shift (Global harmonic)	-5470	-6230	-6050
Energy shift (TGA)	-5740	-6480	-6040

## Energy non-conservation in the single-Hessian extended thawed Gaussian approximation

In the single-Hessian thawed Gaussian approximation,<sup>S13</sup> the potential energy is approximated along the trajectory as

$$V_{\text{SH}}(q, t) = V(q_t) + V'(q_t) \cdot (q - q_t) + \frac{1}{2}(q - q_t)^T \cdot V''_{\text{ref}}(q_{\text{ref}}) \cdot (q - q_t). \quad (1)$$

The time derivative of the total energy (based on  $V_{\text{SH}}$ ) of the extended thawed Gaussian wavepacket is

$$\frac{dE}{dt} = \frac{d}{dt} \langle \phi(t) | \hat{H}_{\text{eff}}(t) | \phi(t) \rangle \quad (2)$$

$$= \langle \phi(t) | \frac{d}{dt} \hat{V}_{\text{SH}}(t) | \phi(t) \rangle \quad (3)$$

$$= \langle \phi(t) | b_t^T \cdot (\hat{q} - q_t) | \phi(t) \rangle \quad (4)$$

$$= 2\text{Re}\{\mu(q_0) \langle \psi(t) | \mu'(q_0)^T \cdot Q_0 \cdot Q_t^{-1} \cdot [(\hat{q} - q_t) \otimes (\hat{q} - q_t)^T] \cdot b_t | \psi(t) \rangle\} \quad (5)$$

$$= \hbar \text{Re}[\mu(q_0) \mu'(q_0)^T \cdot Q_0 \cdot Q_t^\dagger \cdot b_t], \quad (6)$$

where  $b_t := (V''(q_t) - V''_{\text{ref}}(q_{\text{ref}})) \cdot m^{-1} \cdot p_t$ . Equation (3) follows because the thawed Gaussian solves exactly the Schrödinger equation with  $\hat{H}_{\text{eff}} = \frac{1}{2} \hat{p}^T \cdot m^{-1} \cdot \hat{p} + \hat{V}_{\text{SH}}(t)$ . In Eq. (5) we used the fact that the Gaussian probability density  $|\psi(q, t)|^2$  is an even function centered at

$q_t$ , i.e., the integrals of terms that are linear and cubic in  $(q - q_t)$  vanish and in Eq. (6) we used the relation  $\langle \psi(t) | (\hat{q} - q_t) \otimes (\hat{q} - q_t)^T | \psi(t) \rangle = (\hbar/2) Q_t \cdot Q_t^\dagger$  for the position variance in state  $\psi$ .

## Adiabaticity and population dynamics evaluated with different nuclear dynamics methods

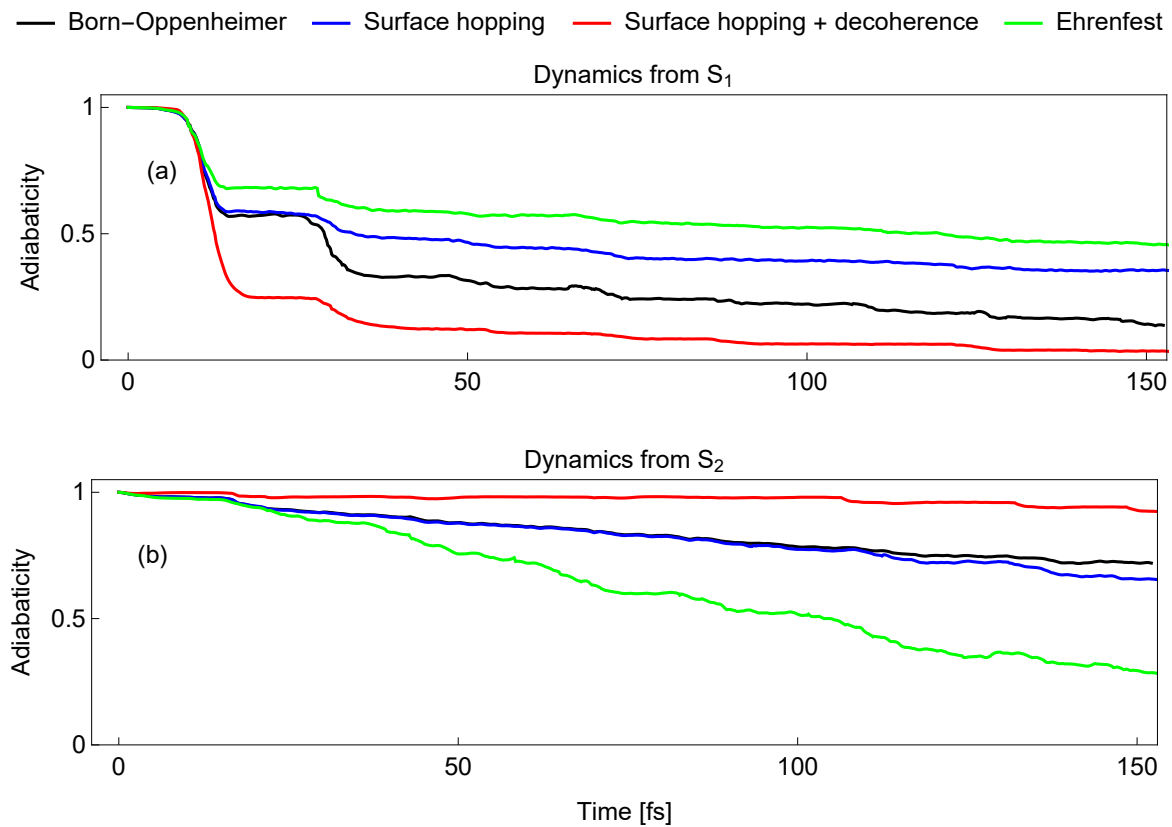


Figure S2: Adiabaticity of the quantum dynamics initiated at the S<sub>1</sub> (upper panel) or S<sub>2</sub> (lower panel) state. Several nuclear dynamics methods are compared.

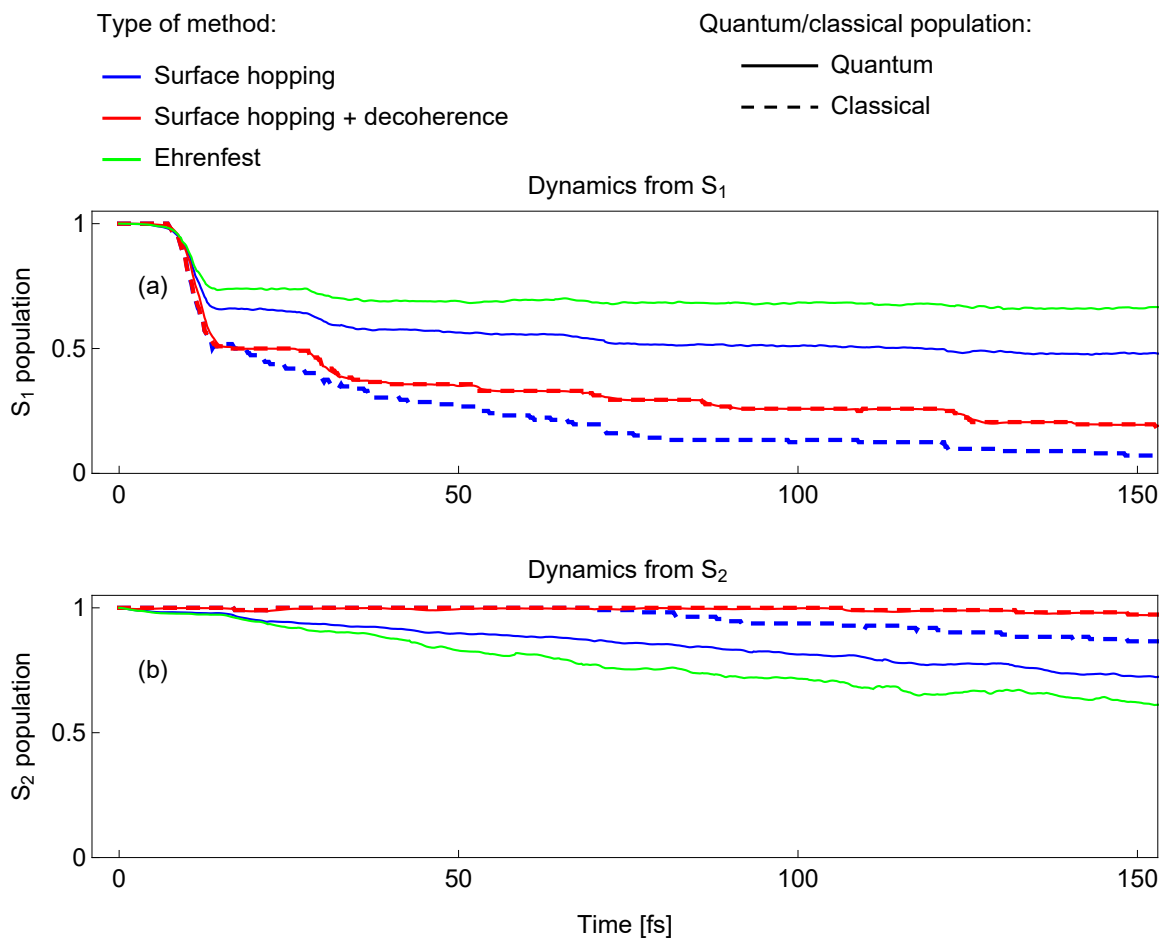


Figure S3: Population of the  $S_1$  state during the dynamics initiated at  $S_1$  (upper panel) and population of the  $S_2$  state during the dynamics initiated at  $S_2$  (lower panel) computed with different nuclear dynamics methods.



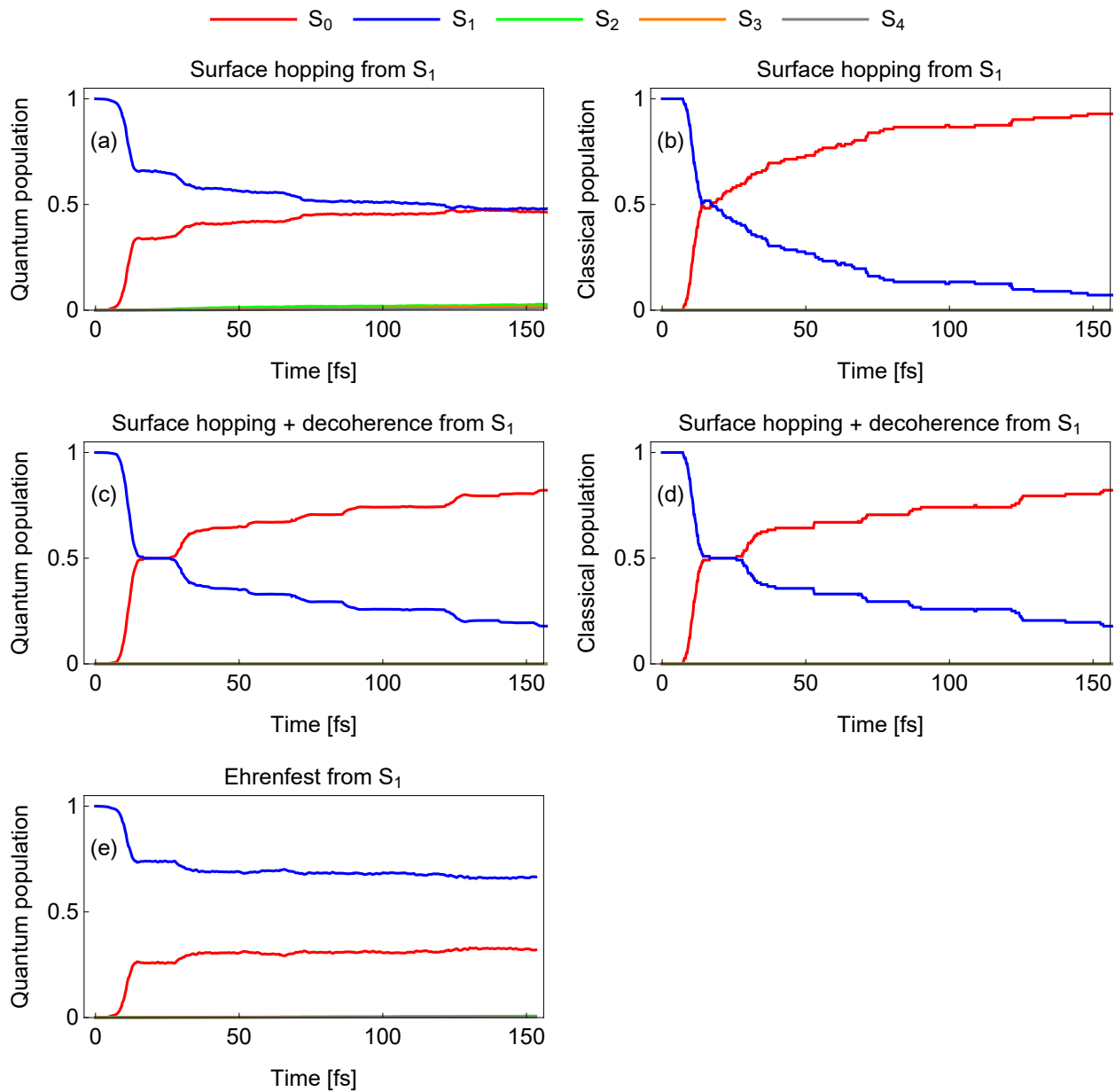


Figure S4: Populations of states  $S_0$ – $S_4$  obtained with different nuclear dynamics simulations initiated at  $S_1$ .

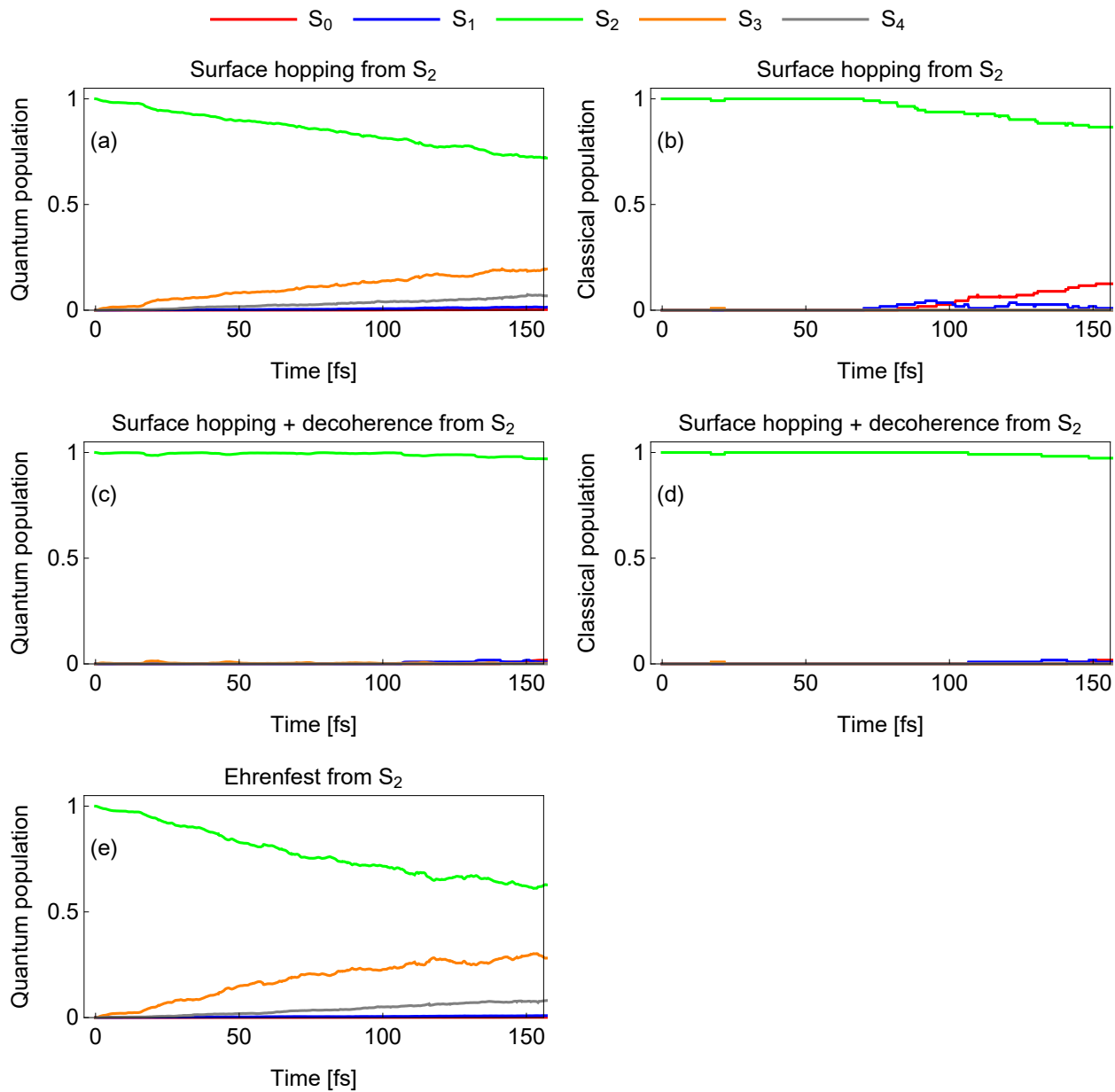


Figure S5: Populations of states  $S_0$ – $S_4$  obtained with different nuclear dynamics simulations initiated at  $S_2$ .

## Adiabaticity divided by initial-state population

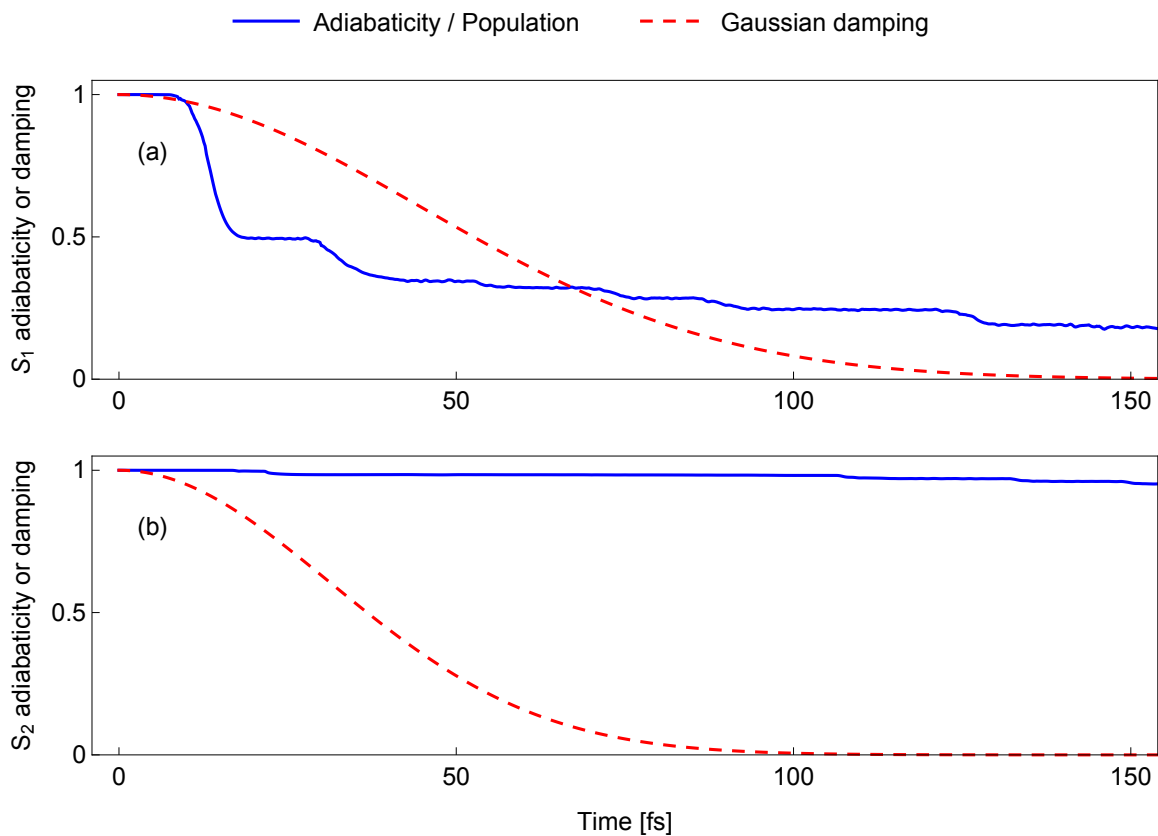


Figure S6: Adiabaticities divided by the initial-state populations (both computed using surface hopping dynamics with decoherence correction, i.e. results shown in Fig. 2 of the main text) for the dynamics started at: (a) S<sub>1</sub>, (b) S<sub>2</sub>. Gaussian decay functions used for broadening the corresponding absorption spectra show the time scales relevant for spectra calculations.

# Asymmetry between $S_2 \leftarrow S_0$ absorption and $S_2 \rightarrow S_0$ emission spectra

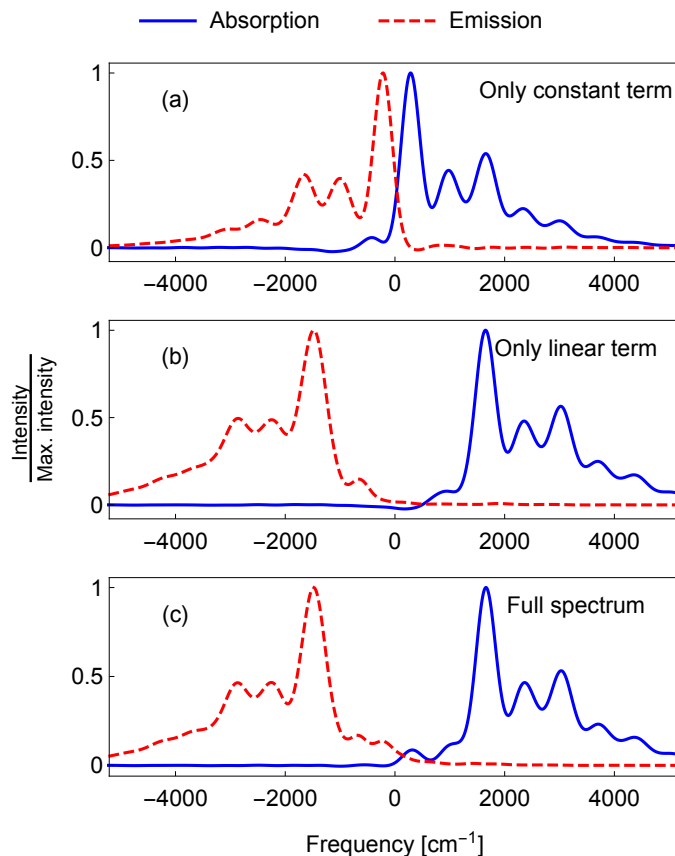


Figure S7: Vibrationally resolved  $S_2 \leftarrow S_0$  absorption and  $S_2 \rightarrow S_0$  emission spectra of azulene computed with (a) only Condon (constant) term, (b) only Herzberg–Teller (linear) term, (c) both Condon and Herzberg–Teller terms in the expansion of the transition dipole moment. Same as Fig. 5 of the main text, but neglecting the Duschinsky rotation between the ground- and excited-state normal mode coordinates, which is accomplished by setting the off-diagonal elements of the reference (adiabatic) Hessian (expressed in the initial-state normal mode coordinates) to zero.

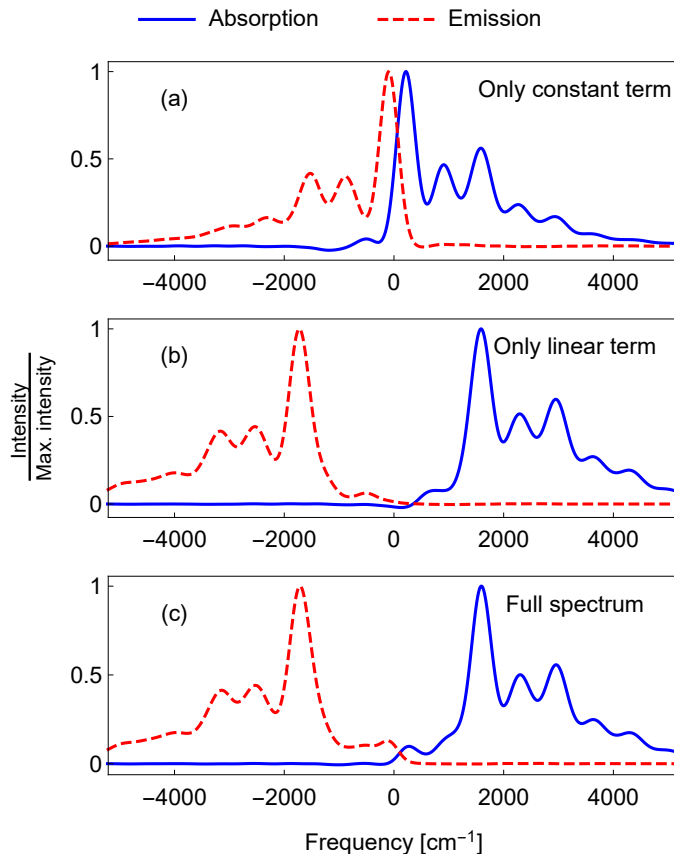


Figure S8: Same as Fig. S7 but here neglecting only the coupling between the Herzberg–Teller active modes (listed in Table S3) in the simulations of the absorption spectra; the emission spectra are the same as in Fig. 5 of the main text.

Table S3: Derivatives of the transition dipole moment (in atomic units) of the azulene  $S_2 \leftarrow S_0$  electronic transition with respect to the normal mode coordinates. Only the largest terms of the transition dipole moment gradient are shown, derivatives with respect to other normal modes are either negligible or zero. The derivatives of the  $z$  component of the transition dipole moment are all zero (the molecule lies in the  $xy$  plane).

Frequency / $\text{cm}^{-1}$	$\partial\mu_x/\partial q \times 10^2$	$\partial\mu_y/\partial q \times 10^2$
1784	−0.86	0.00
1660	−2.50	−5.31
1646	−1.51	0.69
1584	0.00	0.90
1514	1.28	−0.65
1490	1.08	2.32
1409	−0.55	0.00
1235	−0.60	−1.29
1074	0.00	1.05

## References

- (S1) Zimmermann, T.; Vaníček, J. Evaluation of the importance of spin-orbit couplings in the nonadiabatic quantum dynamics with quantum fidelity and with its efficient "on-the-fly" ab initio semiclassical approximation. *J. Chem. Phys.* **2012**, *137*, 22A516.
- (S2) Werner, H.-J.; Knowles, P. J.; Knizia, G.; Manby, F. R.; Schütz, M. Molpro: a general-purpose quantum chemistry program package. *WIREs Comput. Mol. Sci.* **2012**, *2*, 242–253.
- (S3) Werner, H.-J.; Knowles, P. J.; Knizia, G.; Manby, F. R.; Schütz, M.; Celani, P.; Korona, T.; Lindh, R.; Mitrushenkov, A.; Rauhut, G.; Shamasundar, K. R.; Adler, T. B.; Amos, R. D.; Bernhardsson, A.; Berning, A.; Cooper, D. L.; Deegan, M. J. O.; Dobbyn, A. J.; Eckert, F.; Goll, E.; Hampel, C.; Hesselmann, A.; Hetzer, G.; Hrenar, T.; Jansen, G.; Köppl, C.; Liu, Y.; Lloyd, A. W.; Mata, R. A.; May, A. J.; McNicholas, S. J.; Meyer, W.; Mura, M. E.; Nicklass, A.; O'Neill, D. P.; Palmieri, P.; Peng, D.; Pflüger, K.; Pitzer, R.; Reiher, M.; Shiozaki, T.; Stoll, H.; Stone, A. J.; Tarroni, R.; Thorsteinsson, T.; Wang, M. MOLPRO, version 2012.1, a package of ab initio programs. 2012; see <http://www.molpro.net>.
- (S4) Tully, J. C. Molecular dynamics with electronic transitions. *J. Chem. Phys.* **1990**, *93*, 1061–1071.
- (S5) Granucci, G.; Persico, M. Critical appraisal of the fewest switches algorithm for surface hopping. *J. Chem. Phys.* **2007**, *126*, 134114.
- (S6) Dierksen, M.; Grimme, S. Density functional calculations of the vibronic structure of electronic absorption spectra. *J. Chem. Phys.* **2004**, *120*, 3544–3554.
- (S7) Frisch, M. J.; Trucks, G. W.; Schlegel, H. B.; Scuseria, G. E.; Robb, M. A.; Cheeseman, J. R.; Scalmani, G.; Barone, V.; Petersson, G. A.; Nakatsuji, H.; Li, X.;

- Caricato, M.; Marenich, A. V.; Bloino, J.; Janesko, B. G.; Gomperts, R.; Men-  
nucci, B.; Hratchian, H. P.; Ortiz, J. V.; Izmaylov, A. F.; Sonnenberg, J. L.; Williams-  
Young, D.; Ding, F.; Lipparini, F.; Egidi, F.; Goings, J.; Peng, B.; Petrone, A.;  
Henderson, T.; Ranasinghe, D.; Zakrzewski, V. G.; Gao, J.; Rega, N.; Zheng, G.;  
Liang, W.; Hada, M.; Ehara, M.; Toyota, K.; Fukuda, R.; Hasegawa, J.; Ishida, M.;  
Nakajima, T.; Honda, Y.; Kitao, O.; Nakai, H.; Vreven, T.; Throssell, K.; Mont-  
gomery, J. A., Jr.; Peralta, J. E.; Ogliaro, F.; Bearpark, M. J.; Heyd, J. J.; Broth-  
ers, E. N.; Kudin, K. N.; Staroverov, V. N.; Keith, T. A.; Kobayashi, R.; Normand, J.;  
Raghavachari, K.; Rendell, A. P.; Burant, J. C.; Iyengar, S. S.; Tomasi, J.; Cossi, M.;  
Millam, J. M.; Klene, M.; Adamo, C.; Cammi, R.; Ochterski, J. W.; Martin, R. L.;  
Morokuma, K.; Farkas, O.; Foresman, J. B.; Fox, D. J. Gaussian 16 Revision C.01.  
2016; Gaussian Inc. Wallingford CT.
- (S8) Werner, H.-J.; Knowles, P. J.; Knizia, G.; Manby, F. R.; Schütz, M.; Celani, P.;  
Györfy, W.; Kats, D.; Korona, T.; Lindh, R.; Mitrushenkov, A.; Rauhut, G.;  
Shamasundar, K. R.; Adler, T. B.; Amos, R. D.; Bernhardsson, A.; Berning, A.;  
Cooper, D. L.; Deegan, M. J. O.; Dobbyn, A. J.; Eckert, F.; Goll, E.; Hampel, C.;  
Hesselmann, A.; Hetzer, G.; Hrenar, T.; Jansen, G.; Köppl, C.; Liu, Y.; Lloyd, A. W.;  
Mata, R. A.; May, A. J.; McNicholas, S. J.; Meyer, W.; Mura, M. E.; Nicklass, A.;  
O’Neill, D. P.; Palmieri, P.; Peng, D.; Pflüger, K.; Pitzer, R.; Reiher, M.; Shiozaki, T.;  
Stoll, H.; Stone, A. J.; Tarroni, R.; Thorsteinsson, T.; Wang, M. MOLPRO, version  
2015.1, a package of ab initio programs. 2015; see "<http://www.molpro.net>".
- (S9) Kats, D.; Schütz, M. A multistate local coupled cluster CC2 response method based  
on the Laplace transform. *J. Chem. Phys.* **2009**, *131*, 124117.
- (S10) Baiardi, A.; Bloino, J.; Barone, V. General Time Dependent Approach to Vibronic  
Spectroscopy Including Franck-Condon, Herzberg-Teller, and Duschinsky Effects.  
*J. Chem. Theory Comput.* **2013**, *9*, 4097–4115.

- (S11) Patoz, A.; Begušić, T.; Vaníček, J. On-the-Fly Ab Initio Semiclassical Evaluation of Absorption Spectra of Polyatomic Molecules beyond the Condon Approximation. *J. Phys. Chem. Lett.* **2018**, *9*, 2367–2372.
- (S12) Begušić, T.; Patoz, A.; Šulc, M.; Vaníček, J. On-the-fly ab initio three thawed Gaussians approximation: a semiclassical approach to Herzberg-Teller spectra. *Chem. Phys.* **2018**, *515*, 152–163.
- (S13) Begušić, T.; Cordova, M.; Vaníček, J. Single-Hessian thawed Gaussian approximation. *J. Chem. Phys.* **2019**, *150*, 154117.